1960

Electronic applications of magnetic films

Alvin Ashley Read
Iowa State University

ELECTRONIC APPLICATIONS OF MAGNETIC FILMS

by

Alvin Ashley Read

A Dissertation Submitted to the

Graduate Faculty in Partial Fulfillment of

The Requirements for the Degree of

DOCTOR OF PHILOSOPHY

Major Subject: Electrical Engineering

Approved:

Signature was redacted for privacy.

In Charge of Major Work

Signature was redacted for privacy.

Head of Major Department

Signature was redacted for privacy.

Dean of Graduate College

Iowa State University
Of Science and Technology
Ames, Iowa

1960

TABLE OF CONTENTS

I. INTRODUCTION

The purpose of this investigation was to study in both analytical and experimental detail the possible utilization of thin single domain ferromagnetic films of 80-20 permalloy in electronic engineering devices. Such magnetic films have heretofore been limited largely to use in digital computer memory systems although other applications seem economically feasible and practical. This type of thin film was first devised some six or seven years ago. Since then they have been rather extensively studied in an attempt to solve the problems of fabrication ease and of operational speed in digital computer systems. Inasmuch as most of the investigatory studies have been made by computer organizations, it is understandable why many of the noncomputer possibilities have heretofore gone uninvestigated.

Since both the thin magnetic film technique and some of the applications to be investigated are rather new developments which date back only to the last half dozen years or so, this introductory section is divided into two parts, the first part referring to thin film history and properties and the second part referring to the parametric type of applications in which nonlinear reactances are utilized.

A. Magnetism and Thin Films

The films being considered in this thesis are made of a nickel-iron alloy of approximately 80 percent nickel and 20 percent iron. Commonly referred to as 80-20 permalloy, this material is vacuum deposited on thin substrates of glass, mica or plastic although glass is the most common.

The choice of this composition was dictated in part from the unavailability of other types of films and in part from the fact that films of this type possess some very desirable characteristics such as low anisotropy and low magnetostriction coefficients. These films are flat pill box shaped bodies that may vary in shape from being elliptical to being rectangular. Typical films can be in the order of 100 to 10,000 angstroms thick and may have surface areas of several square centimeters. In addition to vacuum deposition, electrodeposition has been studied in some laboratories. Other ratios of constituent materials and even other materials altogether might be useful in accentuating certain properties for specific device applications. Experiments with other types of deposition and with other materials are deemed to be outside the scope of this thesis and, although interesting and potentially very important, will not be considered further in it.

Before discussing the properties of thin ferromagnetic films, a brief discussion of isotropic bulk ferromagnetic material is in order. The term isotropic here means that the material when viewed as a bulk sample has no preferred magnetic directions. When a macroscopic sample of such material is examined in microscopic detail, it is experimentally discovered that it is subdivided into a large number of small regions called magnetic domains, each of which is spontaneously magnetized to saturation. Adjoining domains will have their magnetization in different directions. A "demagnetized" sample of a ferromagnetic material is "demagnetized" only in the sense that the arrangement of the domains within the sample is such that there is a zero net flux for the sample as a whole, i.e., the domains

are so oriented that the magnetic flux circuits lie entirely within the sample. This implies a very high degree of ordering of the domain configurations rather then just any arbitrary random arrangement.

Between one domain and another is a narrow transition region called a domain wall; a domain wall consists of the region where the direction of the magnetic dipoles arising from the spin of ferromagnetic electrons gradually changes from being parallel with the magnetization of one domain to being parallel with the magnetization of the other domain. The width of a domain wall is in the order of a thousand angstroms while the width dimensions of a domain are in the order of several tens of thousand angstroms. The length may be several millimeters or more. For a discussion of the factors which determine these dimensions, the reader is referred to the works of Kittel and others (1-4).

When an external magnetic field is applied to the sample, some of the magnetic dipoles in the domain walls, which are relatively close to a domain whose magnetization vector is more or less parallel with the direction of this external field, tend to align themselves with the domain under the influence of this slightly increased force. At the same time, dipoles close to a domain wall in domains antiparallel to the external field tend to be rotated slightly out of parallel coincidence with their parent domain and to become a part of the domain wall. In this way domain walls tend to move under the influence of external magnetic fields with the domains parallel to the external field growing at the expense of the antiparallel domains. This then gives a net magnetization along the direction of the applied field. This substantially increases the magnetic

flux density over what it would be if the material were not present. This is, for the most part, a low field phenomenum. By the time sufficiently high fields are reached, essentially all the antiparallel domains have been engulfed by the parallel domains. However, a few domains usually remain which were originally perpendicular to the direction of the applied field. The force on the magnetic dipoles in these domains increases as the field increases causing them to tend to rotate and to become parallel to the applied field. Because of crystalline anisotropy, this domain rotation usually requires considerably more force than domain wall movement and as such is a high field phenomenum. Ferromagnetic materials are normally magnetized by a combination of domain wall movements and domain rotations.

When a thin film of 80-20 permalloy is vacuum deposited on a substrate in the presence of an external magnetic deposition field of a few oersteds parallel to the plane of the film, the atomic structure of the film is ordered in such a manner that it possesses an uniaxial anisotropy along an axis parallel to the original direction of the deposition field. Hereafter this direction will be called the "easy" or the "rest" direction of magnetization. The direction normal to the rest direction but still in the plane of the film will be called the "hard" or the "transverse" direction. Later, in discussions relative to the application of these films for device purposes, it is convenient to call these directions the "pump" and the "signal" directions respectively.

When the thickness of the film is less than the dimensions of a normal domain, one would not expect to find a domain wall existing through

the thickness of the film. If a film possessed true uniaxial anistropy, the magnetic moments of the ferromagnetic electrons would have a preferred alignment either parallel to or antiparallel to the easy direction. The application of a small magnetic field along the easy direction would cause any existing domain walls to move until only domains parallel with this field are left. Since this is domain wall movement rather than rotation, removal of the external field should leave the entire film as one single domain. However, with the lateral dimensions of a film being many times a domain dimension, one would expect that it would be fairly easy to cause a thin film in a single domain state to break up into a multiple domain state.

In practice, it is found that the film can actually exist in a multiple domain state or in a nearly single domain state. In the latter instance, there are usually some small parasitic domains around the edges of the films which, in the absence of a bias field, are not aligned along the easy direction of the majority of the film.

In an MKS units system, the vector magnetic flux density $\vec{B}$ in a magnetic domain is given as

$$\vec{B} = \mu_o \vec{H} + \vec{M} \qquad 1$$

where μ_o is the permeability of free space, $\vec{H}$ is the total magnetic field intensity at the point of interest and $\vec{M}$ is the vector saturation magnetization per unit volume of material. For the great majority of applications of interest, the magnitudes of $\vec{M}$ and $\vec{H}$ are such that $M \gg \mu_o H$.

Now if one were to take a reasonably good single domain film and investigate its hysteresis loop characteristic along the easy direction, it is easy to visualize on the basis of the preceding discussion, that one

should expect to observe a square hysteresis loop. Consider, for instance, a magnetic field $\vec{H}$ increasing antiparallel to the magnetization $\vec{M}$ of a good single domain film. At a certain value of $\vec{H}$ and at some point or points in the film such as at discontinuities in the crystalline structure, domains with a magnetization parallel to $\vec{H}$ will nucleate. These domains will then grow very rapidly until all the dipoles in the film have been reversed. To nucleate a domain in the presence of the effective field of the film due to its magnetization requires a substantial external field. Until this value of field is reached there will be no noticeable effect on the film. As soon as it is exceeded, however, a rapid reversal of magnetization takes place giving rise to a square loop hysteresis characteristic. On the other hand, if a transverse direction hysteresis loop is investigated one would expect that rotation would occur so that the characteristic curve should be closed and fairly linear as a function of exciting field strength until the magnetization is rotated parallel to the transverse axis. At this point, the flux density would be a maximum and the material would be saturated in the transverse direction. Hysteresis loop characteristics of these types for good films are fairly easily demonstrated experimentally indicating that the actual film is essentially a single magnetic domain.

The early interest in the magnetic properties of thin films came as a part of an extensive program of investigation of magnetism in general based in part, at least, on the increased engineering application and the demand for magnetic materials with more optimum properties. It had been well known for some time that as one rolled a nickel-iron permalloy tape thinner and thinner its hysteresis loop grew more square. Blois (5) sug-

gested that one could obtain the equivalent of a very thin tape by the evaporation of a permalloy film a few thousand angstroms thick onto a suitable substrate. Kittel earlier had predicted that such a thin film should be able to exist as a single magnetic domain. Blois' success in producing films with good square hysteresis loop characteristics led him to propose the possible use of such a film as a binary data storage element. This led to an intensive program of investigation of thin ferromagnetic films primarily for computer memory applications which is still continuing (6-16).

In investigating the dynamical behavior of thin films under high speed switching and other high frequency excitations, several of these investigators (11-14) refer to a phenomenological theory of rotational processes formulated by Landau and Lifshitz (17) and later modified somewhat by Gilbert (18). Gillette and Oshima's (13) approach to this problem will be utilized later in devising a high frequency model for an inductor with a thin film core.

B. Nonlinear Reactances and Parametric Devices

Concurrent with the materials work described in the preceding paragraphs, considerable effort has been expended in the use of nonlinear reactance elements as modulators, demodulators, mixers and as parametric amplifiers (19-36). When a signal is impressed across an inductance or a capacitor whose value is being periodically varied in time, many new frequencies arise. These new frequencies are involved combinations of the original frequencies and of their harmonics. By proper tuning techniques the power of some of these frequencies can be suppressed while the power

of others allowed to flow. One method of achieving this periodically varying reactance is to impress a large local oscillator "pump" signal across the nonlinear reactance element at the same time as a small signal is applied. Manley and Rowe (35-36) discuss some of the general properties of such systems. They show that, given a system in which both the pump and the signal vary sinusoidally at a frequency of f_p and f_s respectively, one has, for the case where the reactance has no hysteresis, the two independent relations

$$\sum_{m=0}^{\infty} \sum_{n=-\infty}^{\infty} \frac{mP_{m,n}}{mf_p + nf_s} = 0$$

$$\sum_{m=-\infty}^{\infty} \sum_{n=0}^{\infty} \frac{nP_{m,n}}{mf_p + nf_s} = 0. \qquad (2)$$

Here $P_{m,n}$ is the average power input to the reactance at the frequencies $f = \pm|mf_p + nf_s|$. For a detailed analysis of the implications of these relations, the reader is referred to the original articles.

Briefly, however, these relations indicate that a large power gain can be achieved by frequency upconversion from an f_s such that $f_s \ll f_p$ to a new frequency $f_+ = f_p + f_s$ by the interaction of f_s with f_p. They also indicate that when an f_s such that $f_s < f_p$ interacts with f_p to give $f_- = f_p - f_s$, it is possible for both the frequencies f_s and f_- to absorb power from the pump supply. This is what makes a parametric amplifier possible. Of course, instead of f_s and f_p, some harmonic terms of these frequencies might have been used instead. The analysis would have been similar.

In order to function, a parametric amplifier must have power present

at frequencies f_s and f_- as well as at the pump frequency f_p. This then requires that, for efficient operation, tuned circuits be used to minimize circuit reactance and to maximize output power. The system operation, then is such that power is transferred from the pump circuit to the f_s and f_- circuits, usually called the signal and the idler circuits respectively. The power, for instance, transferred into the signal circuit, adds to the power of the signal already there and reinforces it. Thus one has an amplifier. Power gains in the order of 20 decibels are reasonable. If the power input from the pump is increased to the point where more power is supplied to the signal and idler circuits than required to overcome losses, the system will be regenerative and oscillate at two frequencies simultaneously, one frequency near f_s and the other near f_-.

The majority of the devices described to date use the nonlinear voltage-capacitance characteristics of back-biased junction diodes as their nonlinear reactive element. Devices of this type have been made to operate successfully up to frequencies of several kilomegacycles per second. Some devices have also been made that use ferrites. The large volume and large demagnetizing fields of the ferrites used in the devices that have been considered so far necessitates high pump power levels. This appears to make them impractical for extensive application in the area of parametric devices.

Thin films of many magnetic materials which advantageously use the strong demagnetizing fields normal to the plane of the film and at the same time have low internal losses because of small volume show promise for use as nonlinear reactance elements. Details of the latter will be

considerably expanded in later sections of this thesis.

One of the advantages of nonlinear reactance devices is the possibility of relatively low noise operation. Utilized as the first amplifying stages of sensitive microwave or other high frequency receivers, vastly improved system performance is possible. Although not as low noise a device as the maser, it is nevertheless possible to build a receiving system whose receiver noise is at least comparable to the sky noise from an antenna system beamed directly overhead. Some discussions of relative noise measurements are given by Heffner (29, 30) and by Wade (32).

When a degenerate parametric amplifier with only one resonant circuit tuned to $f_s = f_- = f_p/2$ is "pumped hard", the circuit will oscillate at the frequency $f_p/2$. Such an oscillator can be in either one of two stable phase states relative to the pump. Once established in one of these phase states it will remain locked in this phase state until the pump amplitude is lowered to the point where oscillations can no longer be sustained.

A consideration of this phenomenum led von Neuman (37) to propose that such devices could be used in microwave computer systems (38, 39) which he envisioned as operating at millimicrosecond speeds. At the same time Goto (40) in Japan devised a similar but a lower frequency device using ferrite cores which he called a "parametron". This has come to be the accepted name for a phase locked parametric oscillator oscillating at one-half the frequency of the pump. To date several Japanese computers have been constructed using logic circuits containing parametron elements. The highest reported pump frequency (40) is six megacycles per second.

II. INVESTIGATION

A. Derivation of an Inductance Equation for a Thin Film Inductor

1. Quasi-static model formulation of the inductance equation

In this section an expression will be derived giving the inductance value of an inducter using a thin film as a core material. This expression is applicable at low frequencies where quasi-static conditions exist. One starts this derivation with a consideration of the energies that are of practical concern in the theory of domain structures. Kittel and others (1, 2) list four types of energy that are of importance in determining domain structures: Exchange energy; anisotropy energy; magnetoelastic energy; and magnetostatic energy. Of these, magnetoelastic energy can be considered negligible since 80-20 permalloy of which the films being considered in this report are made has a very low magnetostriction coefficient.

The exchange energy is considered to result for the most part from interactions of electron spins. It is this energy which accounts for most of the magnetic characteristics of a material and is the energy which keeps the elementary magnetic dipole moments of the ferromagnetic electrons tightly coupled together so that they all tend to move collectively. Rotation of one spin moment out of parallelism with the rest of the spins requires an expenditure of energy by the rotating agent. Since in a perfect single domain ferromagnetic structure where there are no domain walls, domain rotation is the only mechanism which allows magnetic changes to occur, the exchange energy is a constant independent of

the magnetization orientation with respect to the crystallographic axis.

This leaves only the anisotropy and the magnetostatic energy as the major energy contributions in the case of single domain 80-20 permalloy films. In the discussion of these energies reference should be made to Fig. 1(A). For thin films of the orientation of Fig. 1(A), the anisotropy energy density for 80-20 permalloy films has been found to be of the form

$$W_{aniso} = K \sin^2\phi \cos^2\varphi + K \sin^2\varphi \qquad 3$$

where ϕ is the angle the magnetization vector $\vec{M}$ makes with the rest direction and K is the anisotropy constant of the material.

The magnetostatic energy density which is given by the negative of the scalar product of the total magnetic field intensity and the magnetization vector can be divided into two parts. The first part is due to the interaction of the magnetization $\vec{M}$ with an external applied magnetic field $\vec{h} = \hat{a}_x h_R + \hat{a}_y h_T$ to give in terms of the orientation of Fig. 1(A) a magnetostatic energy of

$$W_{ext} = -\vec{h} \cdot \vec{M} = -h_R M \cos\phi \cos\varphi - h_T M \sin\phi \cos\varphi. \qquad 4$$

Here the $\hat{a}$'s are unit vectors along their respective coordinate axes. The second part of the magnetostatic energy density is due to the magnetization itself in conjunction with the shape factors of the sample inducing demagnetizating fields in the material. In a general case these demagnetizing fields can be expressed in terms of demagnetizing factors N_x, N_y and N_z as

$$\vec{H}_{demag} = (1/\mu_o)(\hat{a}_x N_x M_x + \hat{a}_y N_y M_y + \hat{a}_z N_z M_z) \qquad 5$$

where μ_o is the permeability of free space and the M's are the components of $\vec{M}$ along the indicated axes. For a thin elliptical disc with the orien-

Fig. 1. (A) The schematic representation of a single domain thin film illustrating the coordinate system and applied magnetic fields used in the accompanying analysis

(B) The schematic representation of the thin film paremetric inductor assumed in this thesis and using the film illustrated in (A)

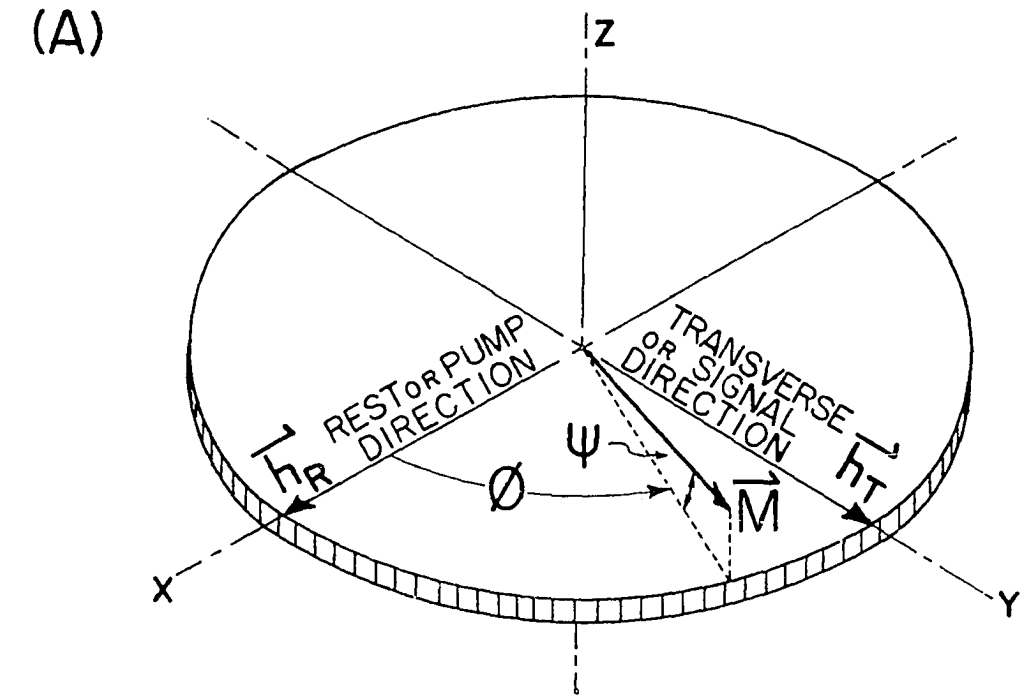
(A)
Z
RESTOR PUMP DIRECTION
TRANSVERSE OR SIGNAL DIRECTION
$\vec{h}_R$
$\vec{h}_T$
Ψ
Ø
$\vec{M}$
X
Y

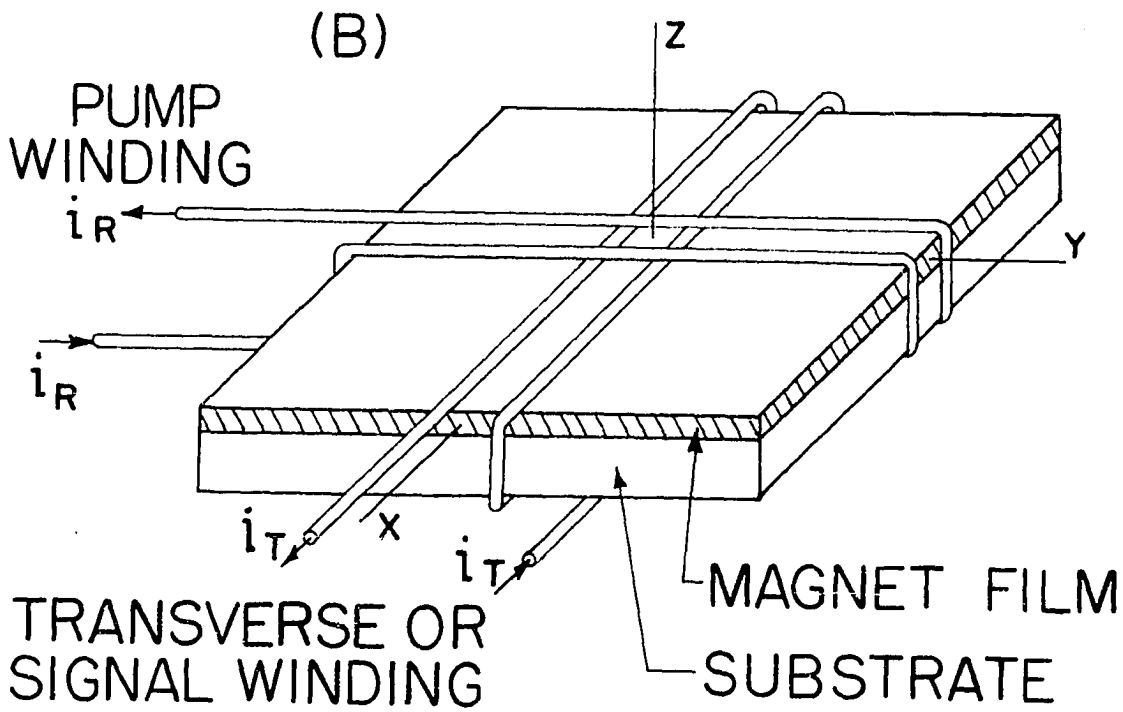
(B)
Z
PUMP WINDING
i_R
Y
i_R
i_T
X
i_T
MAGNET FILM
SUBSTRATE
TRANSVERSE OR SIGNAL WINDING

tation of Fig. 1(A), the demagnetizing factors are $N_x = N_y = 0$ and $N_z = -1$. The factors N_x and N_y remain small even when the actual shape departs appreciably from a pure elliptical shape. Since in this case $M_z = M \sin \varphi$ and with $H_{demag} = -(1/\mu_o)\, M \sin \varphi$, one can write the demagnetizing energy density as

$$W_{demag} = -\vec{H}_{demag} \cdot \vec{M} = (1/\mu_o)\, M^2 \sin^2\varphi. \qquad 6$$

The total magnetic energy density W for a thin single domain 80-20 permalloy film can then be written as

$$W = K \sin^2\phi \cos^2\varphi - h_R M \cos \phi \cos \varphi - h_T M \sin \phi \cos \varphi + (K + M^2/\mu_o) \sin^2\varphi. \qquad 7$$

For given applied fields h_R and h_T, $\vec{M}$ will rotate through the angles ϕ and φ until an equilibrium position is reached which will result in a minimum value for the energy W. One can see immediately from Eq. 7 that, in the lossless quasi-static case being considered here, W will be minimum when $\varphi = 0$. Even at frequencies of several hundred megacycles per second where losses must be considered, the angle φ remains small. With φ very small and still neglecting dynamic losses, the angle ϕ which minimizes W can be found by differentiation of Eq. 7 to give

$$\partial W/\partial\phi = 2K \sin \phi \cos \phi + h_R M \sin \phi - h_T M \cos \phi = 0. \qquad 8$$

Solving Eq. 8 for $\sin \phi$ gives

$$\sin \phi = h_T'/(1 + h_R'/\cos \phi) \qquad 9$$

where one defines $h_T' = h_T M/2K$ and $h_R' = h_R M/2K$.

Equation 9 becomes important when one considers it in conjunction with Fig. 1(A) and with the physical meaning of the magnetization vector $\vec{M}$. Since $N_x = N_y = 0$ and φ is small, the magnetic flux density in the thin

film material can be written using Eq. 1 as

$$\vec{B} = \mu_o\vec{h} + \vec{M} = \hat{a}_x(\mu_o h_R + M \cos \phi) + \hat{a}_y(\mu_o h_T + M \sin \phi). \qquad 10$$

Here $\vec{M}$ can be recognized as the contribution made to the flux density by the presence of the material. In single domain films in the orientation of Fig. 1(A), one can therefore write the component of flux density in the transverse direction as

$$B_T = \mu_o h_T + M \sin \phi. \qquad 11$$

The last term in Eq. 11 is really the intrinsic transverse flux density B_{iT} of the film and can be written in the form of

$$B_{iT}/M = \sin \phi = h_T'/(1 + h_R'/\cos \phi). \qquad 12$$

One can now use Eq. 12 to construct a set of normalized characteristic B-H curves for transverse fields h_T' using h_R' as a parameter. Figure 5(A) shows such a set of curves. These curves will be considered in greater detail later.

The next step in the development of an inductance equation is to suppose that two mutually perpendicular windings are wound around the film as indicated in Fig. 1(B). Call the outer winding with its axis along the rest direction of the film the pump winding and the inner winding with its axis along the transverse direction of the film, the signal or transverse winding. Currents i_R and i_T respectively in these windings will produce fields h_R and h_T in the film. Consider the flux linkage in the transverse winding of Fig. 1(B). If A is the cross-sectional area of the transverse winding, A_m the cross-sectional area of the film, N the number of turns on the transverse winding and if the flux density is reasonably uniform over the cross-section of the film and likewise over the cross-section of the

substrate, one can write, using Eq. 11 and the definition of flux linkage, that

$$\lambda_T = NA\mu_o h_T + NA_m M \sin \phi$$

$$= NA\mu_o h_T + \lambda_m \sin \phi \qquad 13$$

where $\lambda_m = NA_m M$ is the maximum possible flux linkage contribution from the material. For the case where ϕ is small, Eq. 13 reduces to

$$\lambda_T = NA\mu_o h_T[1 + (A_m M h_T'/A\mu_o h_T)/(1 + h_R M/2K)]. \qquad 14$$

The current i_T in the transverse winding and the magnetic field h_T it establishes can be assumed to be related by the expression $h_T = k_T i_T$. Similarly the pump field can be related to the current in the pump winding as $h_R = k_R i_R$. One now finds it convenient to define the new terms α, β and L_o as

$$\alpha = A_m M h_T'/A\mu_o h_T = A_m M^2/A\mu_o 2K,\ \beta = k_R M/2K \text{ and } L_o = NA\mu_o k_T$$

where use has been made of the definitions following Eq. 9. In terms of these defined quantities, which will be used in the remainder of this thesis, Eq. 14 can be written as

$$\lambda_T = L_o i_T[1 + \alpha/(1 + \beta i_R)]. \qquad 15$$

The total inductance of the transverse winding can then be defined and written as

$$L_T = \lambda_T/i_T = L_o[1 + \alpha/(1 + \beta i_R)]. \qquad 16$$

One should take note of the fact that if $i_R = I_b$ is a d.c. current, the product βI_b will always be positive for any but perhaps the very smallest values of I_b. If I_b is of any useable magnitude to serve as, for example, a magnetic bias current, then after a suitable time it will be

found that the magnetization of the film will have aligned itself either slowly or rapidly so that it lies along the direction of $\vec{h}_R$, albeit in the +x or the -x directions of Fig. 1(A). $A + I_b$ in the direction shown in Fig. 1(B) will cause $\vec{M}$ to lie in the +x direction. Reversal of I_b will cause $\vec{M}$ to reverse also. This can be accounted for rather simply in the equations containing M by substituting -M wherever +M appears. Since β has the same sign as M, reversing I_b reverses the sign of β but not the sign of βI_b. This fact will be of importance later in the discussion of the possible stable phase states of a thin film parametron.

It can be seen from Eq. 15 that the flux linkage for small angles of rotation is directly proportional to the current i_T, regardless of the timewise complexity of this current. Thus under the small angle assumption, the inductance of the transverse winding acts as a linear element whose value is dependent upon the instantaneous value of the pump winding current but is independent of any current in the transverse winding.

To check the validity of Eq. 16 in a physical situation, a system such as indicated in Fig. 1(B) was constructed and measurements made of the signal winding inductance as a function of a d.c. bias current I_B in a bias winding in parallel with the pump winding as well as against a current I_b in the pump winding itself. From these data, computations were made for L_o, α and β which would best fit the data obtained to a curve of the form of Eq. 16. Figure 2 shows how well Eq. 16 actually does fit a physical situation. These results show that over a bias current range which gives an inductance variation of more than 80 percent of the maximum

Fig. 2. The transverse winding inductance as a function of d.c. current in the pump winding or in the separate but parallel bias winding of an experimental thin film inductor showing the transverse winding inductance to be of the form $L_T = L_o[1 + \alpha/(1 + \beta i_R)]$

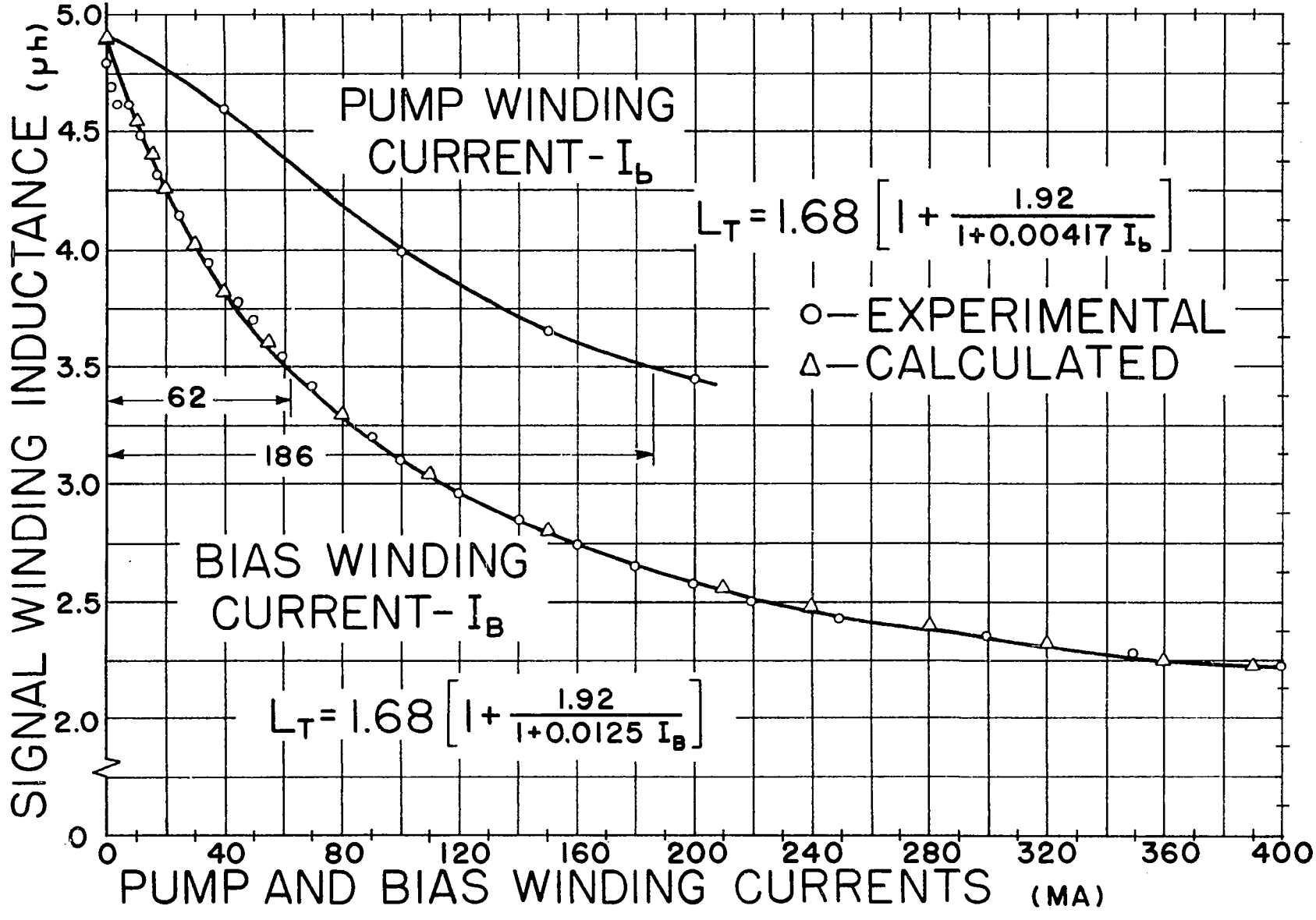
SIGNAL WINDING INDUCTANCE (μh)
5.0
4.5
4.0
3.5
3.0
2.5
2.0
0
PUMP WINDING CURRENT- I_b
$L_T = 1.68\left[1 + \frac{1.92}{1+0.00417\ I_b}\right]$
○—EXPERIMENTAL
△—CALCULATED
62
186
BIAS WINDING CURRENT- I_B
$L_T = 1.68\left[1 + \frac{1.92}{1+0.0125\ I_B}\right]$
0
40
80
120
160
200
240
280
320
360
400
PUMP AND BIAS WINDING CURRENTS (MA)

possible variation, the experimental curve fits almost exactly the theoretically expected shape. Only at very low bias current values where the edges of the film begin to develop small parasitic domains does the experimental curve depart from the expected curve. Measurement of this inductance was made at 7.9 mc/s on a Boonton Radio Corporation Type 160-A Q-meter.

Suppose now that an r.f. current flows in the pump winding and a d.c. current in the bias winding such that an equivalent current for the pump winding can be written as $i_R = I_b + I_p \cos \omega_p t$. Substituting this into Eq. 16 gives the inductance of the transverse winding as

$$L_T = L_o[1 + \alpha/(1 + \beta I_b + \beta I_p \cos \omega_p t)]. \qquad 17$$

Morecroft (41) shows that an expression of the form of Eq. 17 can be expanded into an infinite series as

$$L_T = L_o[1 + a_o/2 + \sum_{n=1}^{\infty} (-1)^n a_n \cos n\omega_p t] \qquad 18$$

where defining

$$\gamma = \beta I_p/(1 + \beta I_b)$$

one lets

$$a_n = \frac{2\alpha}{(1 + \beta I_b)\sqrt{1 - \gamma^2}} \left[\frac{1 - \sqrt{1 - \gamma^2}}{\gamma}\right]^n ;$$

$n = 0, 1, 2, \ldots$.

This definition of a_n insures that it will always have a positive value. Equation 18 shows that current in the pump winding having a sinusoidal component will result in a periodically varying transverse winding inductance having the same fundamental frequency as the pump as well as higher har-

monic terms. Figure 3 shows how the coefficients a_n of Eq. 16 vary as a function of the pump amplitude parameter γ. It is to be noted that the harmonic terms are small until relatively large values of pump current amplitudes are reached. This factor is of importance when any harmonic upconversion techniques or very high frequency operation under high bias conditions are to be considered.

Equation 16 gives an expression for the inductance of an inductor using a thin film as core material. Equation 18 gives a more restricted expression of inductance, being valid only for the case of a d.c. plus a sinusoidal pump winding current. The next step is to compare the quasi-static approach of this section with a dynamic model approach using the phenomenological theory of Landau and Lifshitz (17) as modified by Gilbert (18).

2. Dynamic model formulation of the inductance equation

In this section consideration will be given to a dynamic model of a thin film inductor in which losses are considered as well as the precessing characteristics of the electron spins at frequencies near spin resonance. Starting with Eq. 13 as a good approximation for the flux linkage in the transverse winding for small values of φ, the relations $h_T = k_T i_T$ and $\lambda_m = NA_m M$ as before one can write

$$\lambda_T = \mu_o k_T NA i_T + \lambda_m \sin \phi = L_o i_T + \lambda_{iT} \qquad 19$$

where $L_o = \mu_o k_T NA$ as previously and where $\lambda_{iT} = \lambda_m \sin \phi$ is the intrinsic transverse flux linkage. The voltage induced in the transverse winding can then be obtained as

$$e_T = d\lambda_T/dt = L_o di_T/dt + \lambda_m d(\sin \phi)/dt. \qquad 20$$

Fig. 3. The coefficients of the time-varying components of the transverse winding inductance as a function of the pump amplitude parameter γ

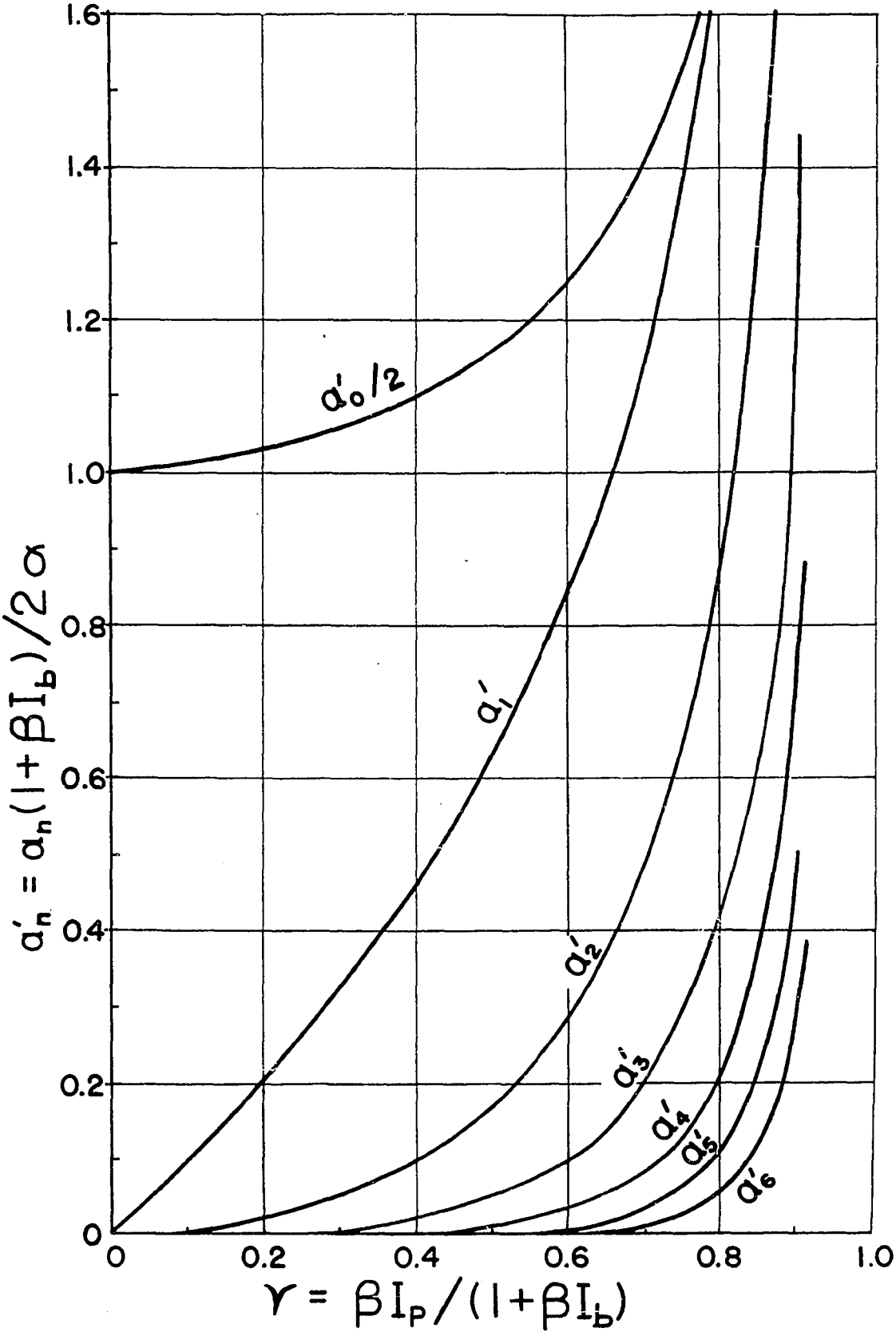
1.6
1.4
1.2
1.0
0.8
0.6
0.4
0.2
0
0
0.2
0.4
0.6
0.8
1.0
$a'_n = a_n(1+\beta I_b)/2\alpha$
$\gamma = \beta I_p/(1+\beta I_b)$
$a'_0/2$
a'_1
a'_2
a'_3
a'_4
a'_5
a'_6

Equation 20 illustrates that the induced voltage in the transverse winding can be broken up into two independent parts, the first part being the voltage across an equivalent air inductance having a value equal to that of the transverse winding in the absence of any magnetic material in the core. The second part is due to the presence of magnetic material in the core. Thus the first part of the equivalent circuit of a thin film inductor is a series inductance L_o.

Before the second part of the equivalent circuit can be determined, the dynamic behavior of the rotation angle ϕ must be determined. The starting point is the Landau-Lifshitz equation as modified by Gilbert (18) which may be written in MKS units as

$$\vec{dM}/dt = -\gamma(\vec{M} \times \vec{H}) + (\delta/M)(\vec{M} \times \vec{dM}/dt). \qquad 21$$

In Eq. 21 $\vec{M}$ is the saturation magnetization vector per unit volume as before, $\gamma = \mu_o g|e|/2m$ is the magnitude of the gyromagnetic ratio of a ferromagnetic electron, δ is the phenomenological damping constant and $\vec{H}$ is the total effective magnetic field in the sample.[1] Before proceeding further make the assumptions that the external fields and the maximum angular frequency ω_{max} of interest are such that the following conditions hold:

(a) $\varphi \ll 1$

(b) $\mu_o 2K/M^2 \ll 1$; $\mu_o h_R/M \ll 1$; $\mu_o h_T/M \ll 1$

(c) $\mu_o \omega_{max}/M\gamma \ll 1$.

---

[1] For permalloy material approximate values of these constants are $\gamma \simeq 221$ kilocycles per second per ampere turn per meter, $\delta \simeq 0.02$ and $M \simeq 0.8$-1.0 webers per square meter.

These assumptions are not particularly restrictive but are quite useful in simplifying some of the analytical expressions to be obtained later.

Gillette and Oshima (13) show that for a single domain thin sheet with the orientation and exciting fields of Fig. 1(A), the equation of motion of the magnetization vector $\vec{M}$ can be reduced to two scalar equations in the rotation angles ϕ and φ. In an equivalent form, their equations can be written as

$$d\phi/ds + \varphi/\mu_o + (\delta/M^2)[\partial W/\partial\phi|_{\varphi=0}] \simeq 0 \qquad 22$$

and

$$d\varphi/ds + \delta\varphi/\mu_o - (1/M^2)[\partial W/\partial\phi|_{\varphi=0}] \simeq 0 \qquad 23$$

where $\partial W/\partial\phi|_{\varphi=0} = 2K \sin\phi\cos\phi + h_R M \sin\phi - h_T M \cos\phi$ and $s = \nu M/(1+\delta^2)t$. It is to be recalled that the term $\partial W/\partial\phi|_{\varphi=0}$ is the quantity equated to zero in Eq. 8 for the quasi-static case where φ was assumed to be zero. To separate Eqs. 22 and 23 to obtain an expression in ϕ only, one can take the derivative d/ds of Eq. 22, multiply the result by μ_o and add this to δ times Eq. 22. If this result is added to the negative of Eq. 23, one then obtains

$$\frac{d^2\phi}{ds^2} + \frac{\delta}{\mu_o}\frac{d\phi}{ds} + \frac{1+\delta^2}{\mu_o M^2}\left[\frac{\partial W}{\partial\phi}\bigg|_{\varphi=0}\right] + \frac{\delta}{M^2}\frac{d}{ds}\left[\frac{\partial W}{\partial\phi}\bigg|_{\varphi=0}\right] = 0. \qquad 24$$

When one performs the derivative indicated by the last term of Eq. 24, it is found that, within the limitations imposed by assumptions (b) and (c) above, this term can be neglected since it is found to be very much smaller than the remaining terms of Eq. 24. Equation 24 then reduces to

$$\frac{d^2\phi}{ds^2} + \frac{\delta}{\mu_o}\frac{d\phi}{ds} + \frac{1+\delta^2}{\mu_o M^2}[2K \sin\phi\cos\phi + h_R M \sin\phi - h_T M \cos\phi] = 0. \qquad 25$$

This can be rewritten as

$$\frac{d^2\phi/ds^2}{\cos\phi} + \frac{\delta}{\mu_o}\frac{d\phi/ds}{\cos\phi} + \frac{2K(1+\delta^2)}{\mu_o M^2}\left[1 + \frac{h_R M/2K}{\cos\phi}\right]\sin\phi = \frac{1+\delta^2}{\mu_o M} h_T. \qquad 26$$

Introducing the new variable $y = \sin\phi = \lambda_{i_T}/\lambda_m$, one has then that $\cos\phi = (1 - y^2)^{1/2}$, $dy/ds = (d\phi/ds)\cos\phi$, and $d^2y/ds^2 = (d^2\phi/ds^2)\cos\phi - (d\phi/ds)^2 \sin\phi$. Therefore upon solving for $d\phi/ds$ and $d^2\phi/ds^2$ in terms of y, dy/ds and d^2y/ds^2, one can upon substituting these into Eq. 26 obtain

$$\frac{d^2y/ds^2}{1-y^2} + \frac{\delta}{\mu_o}\frac{dy/ds}{1-y^2} + \frac{y(dy/ds)^2}{(1-y^2)^2} + \frac{2K(1+\delta^2)}{\mu_o M}\left[1 + \frac{h_R M/2K}{(1-y^2)^{1/2}}\right] y = \frac{1+\delta^2}{\mu_o M} h_T. \qquad 27$$

Since the demagnetizing factors N_x and N_y are essentially zero for the film shapes of interest here, the demagnetizing fields in the plane of the film are very small. Therefore the instantaneous magnetic fields in the film arise primarily from the instantaneous currents i_T and i_R flowing in the transverse and pump windings. As was done previously for the quasi-static case, these fields may be written to a good approximation as $h_T = k_T i_T$ and $h_R = k_R i_R$. If these and the expression for real time t are substituted into Eq. 27 one obtains after some minor rearrangement

$$\frac{\mu_o(1+\delta^2)}{k_T \nu^2 M}\frac{d^2y/dt^2}{1-y^2} + \frac{\delta}{k_T \nu}\frac{dy/dt}{1-y^2} + \frac{\mu_o(1+\delta^2)}{k_T \nu^2 M}\frac{y(dy/dt)^2}{(1-y^2)^2} + \frac{2K}{k_T M}\left[1 + \frac{k_R M i_R}{2K(1-y^2)^{1/2}}\right] y = i_T. \qquad 28$$

From the definition of y and from the far right hand term of Eq. 28 one sees that the term $\lambda_m \, dy/dt = \lambda_m \, d(\sin \phi)/dt$ denotes an induced voltage in the transverse winding. In this light Eq. 28 can be interpreted as a node voltage equation for a parallel RLC circuit. It is to be noted that all these equivalent circuit components are nonlinear. It is also to be noted that under a small angle of rotation assumption such as that previously made in the quasi-static development, the inductance part of this parallel circuit is identical to the term in Eq. 14 for the film component of the quasi-static inductance.

If Eq. 28 is to be interpreted as a node voltage equation then it is convenient to define the small signal electrical circuit parameters $C_o = \mu_o(1 + \delta^2)/\lambda_m k_T V^2 M$, $G_o = \delta/\lambda_m k_T V$ and $\alpha L_o = 2K/\lambda_m k_T M = 2K/NA_m M^2 k_T$ along with the quantities α, β and L_o defined previously following Eq. 14. In terms of these small signal parameters, Eq. 28 can be written in the more simple form

$$C_o\lambda_m \frac{y''}{1 - y^2} + G_o\lambda_m \frac{y'}{1 - y^2} + C_o\lambda_m \frac{y(y')^2}{(1 - y^2)^2} + \frac{\lambda_m}{\alpha L_o}\left[1 + \frac{\beta i_R}{(1 - y^2)^{1/2}}\right] y = i_T \qquad 29$$

where $y' = dy/dt$ and $y'' = d^2y/dt^2$.

Figure 4 shows the equivalent circuit implied by Eq. 29. The various currents through the nonlinear elements are shown. It is assumed that most of the interwinding capacitance effects can be accounted for by the placement of an equivalent capacitance across the terminals of the inductor.

The preceding derivation of Eq. 29 assumed that rotational processes

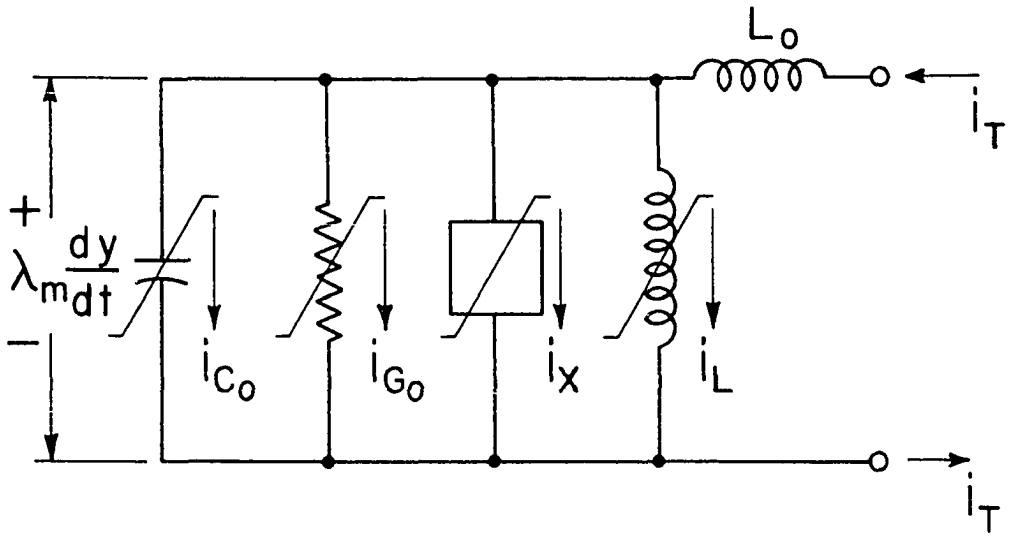

$$i_{C_o} = \frac{\lambda_m C_o}{1 - y^2} \frac{d^2y}{dt^2}$$

$$i_{G_o} = \frac{\lambda_m G_o}{1 - y^2} \frac{dy}{dt}$$

$$i_x = \frac{\lambda_m C_o y}{(1 - y^2)^2} \left(\frac{dy}{dt}\right)^2$$

$$i_L = \frac{1}{\alpha L_o}\left[1 + \frac{\beta i_R}{\sqrt{1-y^2}}\right] \lambda_m y$$

$$y = \frac{\lambda}{\lambda_m}$$

Fig. 4. The equivalent circuit for the dynamic model of the thin film inductor as viewed from the terminals of the transverse winding

alone were occurring in the film. In practice the magnetization appears to rotate homogeneously for moderate angles of rotation. Olson and Pohm (11) give an angle in the order of 60 degrees as the approximate limit for essentially homogeneous rotation. For angles in excess of this, nonhomogeneous effects set in which are not included in the Landau-Lifshitz model used in deriving the equivalent electrical circuit of Fig. 4. Olson and Pohm suggest that this nonhomogeneous effect might arise either from the film completing its rotation one segment at a time or by a continuation of the homogeneous rotation but with an increased damping factor as the angle increases. No attempt will be made here to include these additional large angle effects in the dynamic equation of a thin film inductor. However, it must be realized that any results obtained from the equivalent circuit of Fig. 4 which indicate rotation angles in excess of approximately 60 degrees would in reality be modified by the presence of these nonhomogeneous effects.

B. Thin Film Inductors as Parametrons

One of the simplest circuit configurations in which to use a thin film inductor is as a phase locked subharmonic oscillator, i.e., as a parametron. All that is really required is a tuning capacitor across the terminals of the transverse winding to tune the transverse circuit to approximately one-half the pump frequency and a sinusoidal source of pump current of the proper amplitude. The parametron operation using thin film inductors will be discussed using two different approaches, one approach using a graphical analysis and being quite qualitative and the other being

analytical and much more quantitative but lacking the elementary simplicity of the first.

1. A graphical approach to the thin film parametron

In a previous section, it was stated that one could use Eq. 12 to construct a set of normalized characteristic B-H curves for the transverse field using h_R' as a parameter. Such a set of curves is shown in Fig. 5 (A). If h_R and h_T are simultaneously known, the specific state of the intrinsic flux density can easily be found from Fig. 5(A). Thus, if h_R and h_T are time varying functions, then, as they vary, they will trace out a path in the B-H plane of Fig. 5(A). If h_R and h_T are not simply related, it is evident that this path can become very complex making any graphical considerations quite impractical. The parametron case, however, is quite amiable to a graphical approach. In this case the pump frequency is exactly twice the signal frequency. For a qualitative discussion of this case consider a $h_R = H_p \cos 2\omega t$ and a $h_T = H_T \sin(\omega t + \theta)$ to exist. In a practical situation a d.c. bias field parallel with h_R would undoubtedly be present but for simplicity assume it to be zero. The qualitative results are not affected by its absence. Shown on Fig. 5(A) are the paths followed around the B-H plane for two different values of pump amplitude for the case where the phase angle $\theta = 45$ degrees. It is to be noted that, except for the fact these paths are wasp-waisted, they resemble normal hysteresis loops. The paths followed are counter clockwise such that the area enclosed always lies to the left as is usual for ordinary hysteresis loops. Conventionally, the area contained within a hysteresis loop taken in the counter clockwise sense is interpreted to be the positive energy

Fig. 5 (A) The normalized transverse direction magnetic characteristics of an ideal single domain thin film as a parametric function of the normalized rest direction magnetic field

(A-D) Some possible hysteresis loop examples for a transverse winding current with a frequency that is exactly one-half the frequency of the pump winding current

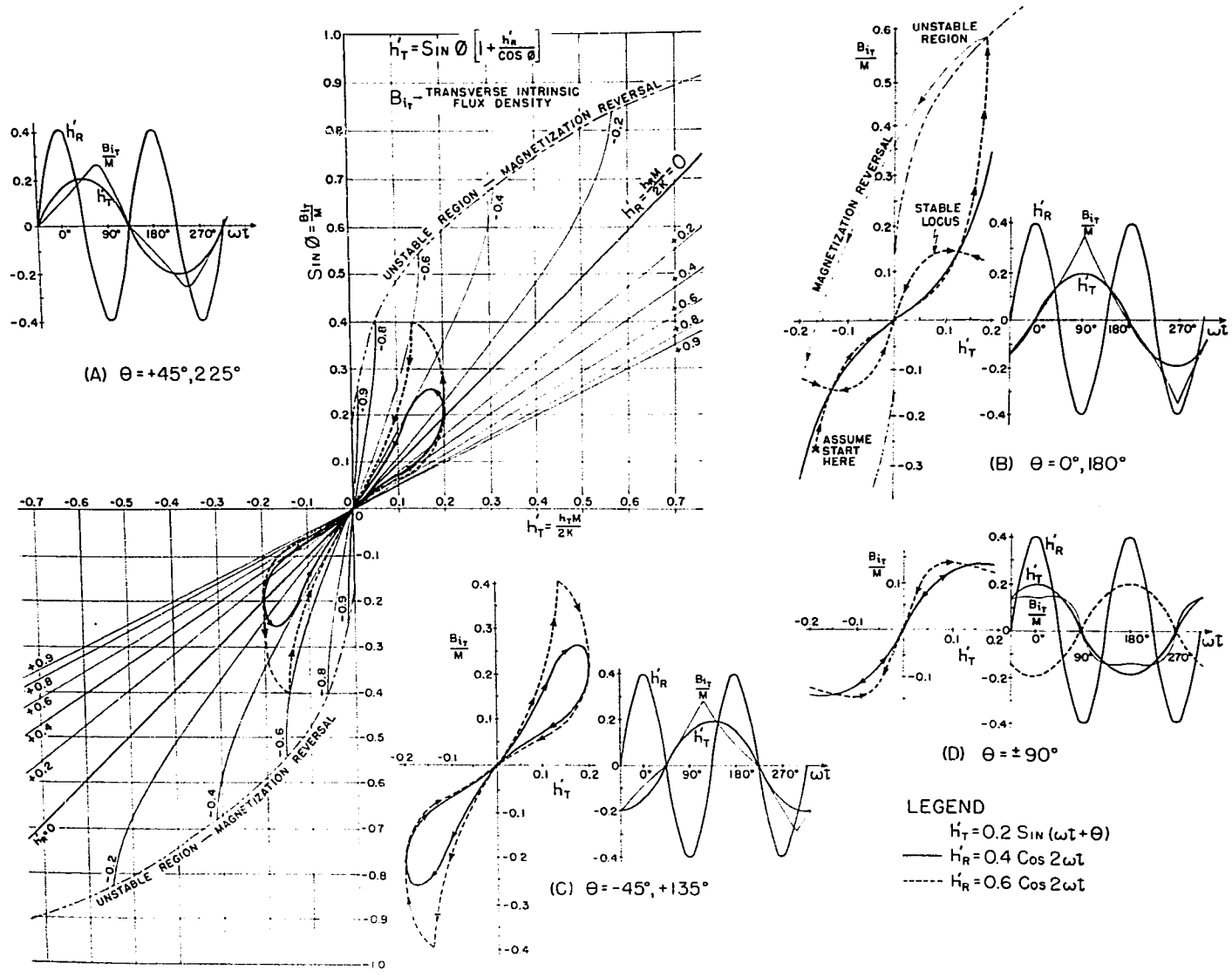
$h'_T = \sin\phi \left[1 + \frac{h'_R}{\cos\phi}\right]$
B_{i_T} – TRANSVERSE INTRINSIC FLUX DENSITY
$\sin\phi = \frac{B_{i_T}}{M}$
$h'_T = \frac{h_T M}{2K}$
$h'_R = \frac{h_R M}{2K} = 0$
UNSTABLE REGION — MAGNETIZATION REVERSAL
UNSTABLE REGION
MAGNETIZATION REVERSAL
STABLE LOCUS
ASSUME START HERE
(A) θ = +45°, 225°
(B) θ = 0°, 180°
(C) θ = -45°, +135°
(D) θ = ± 90°
LEGEND
$h'_T = 0.2 \sin(\omega t + \theta)$
$h'_R = 0.4 \cos 2\omega t$
$h'_R = 0.6 \cos 2\omega t$

supplied per cycle by the exciting current source, in this instance, the transverse current source.

As the phase angle θ decreases toward zero but with the amplitudes of the two fields remaining fixed, the area contained within the hysteresis loop will still be positive but will gradually reduce in value until at $\theta = 0$, the enclosed area will be zero. This situation is illustrated by the solid lined curve in Fig. 5(B). As the phase angle θ goes negative, the area again increases in value. When $\theta = -45$ degrees, as shown in Fig. 5(C), it is to be noted that the curves are identical in shape to those of Fig. 5(A) but that the path of travel is now clockwise. Whereas a counter clockwise path around a hysteresis loop is interpreted as energy being supplied by the signal circuit to the magnetic material, a clockwise path is interpreted as energy being supplied to the signal circuit by the material and its power source, the pump circuit.

As θ goes still more negative, the area once again decreases to zero as shown in Fig. 5(D) for the case when $\theta = \pm 90$ degrees.

In all cases of Fig. 5 the dashed curves illustrate the effect of increasing pump amplitude. In most cases the result is a new stable loop somewhat larger than the previous one. In the case of Fig. 5(B), however, increasing pump amplitude drives the film into the unstable region where the direction of the magnetization reverses. The effect of this is the same as assuming that the magnitude of the magnetization of Fig. (A) to be negative. Then both h_R' and h_T' in Fig. 5(B) switch from negative to positive values at the instant the loop enters the unstable region. A new loop will then be traced out in the B-H plane. This new loop will have

exactly the same shape as that of Fig. 5(D) and will be stable.

When one examines the timewise variation of the transverse flux density as illustrated in Fig. 5, it is noted that in each case the fundamental frequency component is the same as that of the signal frequency while all higher order components are odd harmonics. Thus the voltage induced in the transverse winding will have a component at the frequency of the input current. If one examines this in detail, it is discovered that the input impedance of the transverse winding as seen by the transverse current circuit contains both an inductive and a resistive component. In the case of Fig. 5(A), this resistive component is positive but in the case of Fig. 5(C) it is negative. The magnitude of this input resistance is for the most part dependent upon the amplitude of the pump current and to a much lesser extent upon the transverse signal current.

Any linear signal source can be represented as an ideal voltage source in series with a generator impedance. If such a source is connected to the terminals of the transverse winding, the total resistance around the complete circuit will either be greater or less than the resistance of the generator impedance alone, depending upon the relative phase between the signal and the pump currents. If the reactance of the generator impedance is capacitive so that it tunes out the inductive reactance of the transverse winding, the total resistance around the circuit will determine the current flow in the signal circuit. If the phasing of the signal current results in a negative input resistance, current amplification of the signal current can occur. As the magnitude of this negative resistance approaches the magnitude of positive resistance this amplifi-

cation increases without limit until the point is reached where the negative resistance equals or exceeds the positive resistance. At this point self-sustaining oscillations at one-half the pump frequency begin which grow in amplitude until limited by a combination of losses and detuning phase shifts in the pump and signal circuits. Such a system is, of course, a phase-locked subharmonic oscillator, potentially useful in addition to being a parametron computer logic element as a superregenerative radio frequency detector. A discussion of the latter will be made later.

The preceding qualitative discussion illustrates how the presence in the signal circuit of the signal of proper frequency and phase can cause energy to be supplied by the pump at the correct frequency and phase to reinforce this signal. Improper phasing can likewise result in a loss of signal power. The great dependence of signal gain (or loss) on the relative phase angle θ is quite clearly illustrated.

One could now logically attempt to consider the case of multiple currents flowing through the transverse winding and multiple tuned circuits graphically. This, however, would prove to be quite cumbersome and, inasmuch as the preceding discussion has been qualitative rather than quantitative, much more can be gained from a more analytical approach.

2. An analytical approach to the thin film parametron

A parametron is, as previously discussed, a subharmonic oscillator phase-locked with respect to its a.c. power source. Since it is an oscillator, one is interested in understanding the conditions under which oscillations will occur and what factors determine the oscillation amplitude and phase. Any attempt to study these effects should start with the best model

of the system available. Inasmuch as the model of a thin film inductor based on the Landau-Lifshitz equation is much better than the quasi-static model, the equivalent circuit of Fig. 4 should be considered as a starting point. Assume that an external capacitance C and a conductance G are placed in parallel across the terminals of the circuit of Fig. 4. It is immediately apparent that this system is exceeding complex from an analytical point of view since four of the seven elements in the equivalent circuit of the parametron are nonlinear.

a. The "linearized" parametron equation In order to reduce the complexity of the analytical problem certain simplifying assumptions can be made. First it can be assumed that the film is sufficiently biased by a d.c. magnetic field parallel to the pump field so that the spin resonance of the ferromagnetic electrons occurs at a frequency very much higher than any frequency of interest in parametron operation. This biasing is most easily accomplished by a d.c. component of current in the pump winding. Secondly one can assume that the series inductance L_o is small compared to the inductance due to the film and that the effect of any small series inductance will be only to slightly modify the values of C and G that must be used in an actual system to operate in the manner predicted by the analysis. Third, one can assume that the angle of rotation of the magnetization vector remains considerably less than 90 degrees.

Under the assumptions of the preceding paragraph, the equivalent circuit of the parametron reduces to a single nodal circuit. The assumption concerning frequencies requires that the externally added capaci-

tance C be much greater than C_o. The effective capacitance of the equivalent circuit then contains only a very small nonlinear component and can be considered for all practical purposes as being linear. Likewise, if the externally added conductance G is very much larger than the conductance due to the film, the effective conductance of the equivalent circuit can be considered to be linear. The only nonlinear term remaining in the equivalent circuit is that of the inductance. These assumptions reduce the equivalent circuit of the thin film parametron to that shown in Fig. 6.

The node voltage equation for the equivalent circuit of Fig. 6 is

$$Cy'' + Gy' + \frac{1}{\alpha L_o}\left[1 + \frac{\beta i_R}{(1 - y^2)^{1/2}}\right] y = 0 \qquad 30$$

where $y' = dy/dt$ and $y'' = d^2y/dt^2$. If it is now assumed that

$$i_R = I_b + \sum_{r=1}^{\infty} I_{2r} \cos 2r\omega t \qquad 31$$

then Eq. 30 can be written as

$$y'' + \frac{G}{C}y' + \frac{1 + \beta I_b}{\alpha L_o C}\left[\frac{1}{1 + \beta I_b} + \frac{\Gamma + \sum_{r=1}^{\infty} \gamma_{2r} \cos 2\omega t}{(1 - y^2)^{1/2}}\right] y = 0 \qquad 32$$

where Γ and γ are defined as the bias and the pump parameters respectively by the expressions

$$\Gamma = \frac{\beta I_b}{1 + \beta I_b} \text{ and } \gamma_{2r} = \frac{\beta I_{2r}}{1 + \beta I_b}.$$

If a change of variable is made in Eq. 32 by letting $\omega t = x$ and if the

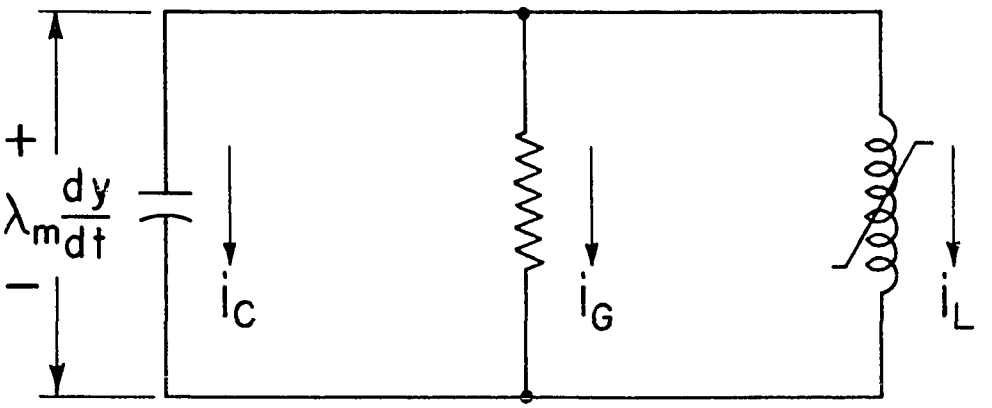

$$i_C = \lambda_m C \frac{d^2y}{dt^2}$$

$$i_G = \lambda_m G \frac{dy}{dt}$$

$$i_L = \frac{1}{\alpha L}\left[1 + \frac{\beta i_R}{\sqrt{1-y^2}}\right] \lambda_m y$$

$$y = \frac{\lambda}{\lambda_m}$$

Fig. 6. The equivalent circuit of a "linearized" thin film parametron

quantities ω_o^2, Q and Q_o are defined as

$$\omega_o^2 = \frac{1 + \beta I_b}{aL_oC}, \text{ and } Q = \frac{G}{\omega C} = \frac{\omega_o}{\omega} Q_o$$

then, upon dividing through by ω^2, Eq. 32 becomes

$$y'' + \frac{\omega_o}{\omega Q_o} y' + \left(\frac{\omega_o}{\omega}\right)^2 \left[\frac{1}{1 + \beta I_b} + \frac{\Gamma + \sum_{r=1}^{\infty} \gamma_{2r} \cos 2rx}{(1 - y^2)^{1/2}}\right] y = 0 \qquad 33$$

where y is now y(x). Although suitable for certain numerical calculations, Eq. 33 is still too complex for easy analytical investigations. Before any simplifications are made, however, it should be noted that if Y(x) is a solution of Eq. 33, then -Y(x) is also a solution. However, because of the periodicity of the pump current $-Y(x) = Y(x \pm \pi)$. Since it will be important later, one should also consider the question of reversing the algebraic sign of the γ_{2r}'s corresponding to odd values of r. This is equivalent to substituting $x = x' + \pi/2$ into Eq. 33. Then if $\pm Y(x)$ are solutions of Eq. 33, then $\pm Y(x') = \pm Y(x + \pi/2) = Y(x \pm \pi/2)$ will be solutions of the new equation. Primary interest is concerned with the case where r = 1. In such a case reversal of the sign of $\gamma_2 = \gamma$ can be accomplished in either of two ways, the first being simply to reverse the phase of the pump current by 180 degrees. The second method involves simply the reversal of the d.c. bias current I_b or the equivalent provided I_b is of sufficient magnitude to cause the film to "flip", i.e., to rotate its rest magnetization direction by 180 degrees. As discussed earlier, this changes the sign of β leaving the product βI_b unaltered but changing

the sign of βI_p and hence of γ.

b. The Hill-Mathieu approximation of the parametron equation If the maximum value of y is restricted to reasonably small values compared to its maximum possible value of unity, then to a good approximation one can write

$$(1 - y^2)^{-1/2} = 1 + (1/2)y^2 + (3/8)y^4 \qquad 34$$

in which case the differential equation of the parametron at low amplitudes can be written as

$$y'' + (\omega_o/\omega Q_o)y' + (\omega_o/\omega)^2\left[\left[1 + \sum_{r=1}^{\infty} \gamma_{2r} \cos 2rx\right] y + \left[\Gamma + \sum_{r=1}^{\infty} \gamma_{2r} \cos 2rx\right]\left[(1/2)y^3 + (3/8)y^5\right]\right] = 0. \qquad 35$$

At extremely low amplitudes of y all terms in y except the first can be neglected leaving

$$y'' + (\omega_o/\omega Q_o)y' + (\omega_o/\omega)^2 \left[1 + \sum_{r=1}^{\infty} \gamma_{2r} \cos 2rx\right] y = 0. \qquad 36$$

If one makes another change of variable

$$y = z \exp\left[-(\omega_o x/2\omega Q_o)\right] \qquad 37$$

then Eq. 36 can be rewritten in the form of a Hill's equation as

$$z'' + (\omega_o/\omega)^2 \left[1 - (1/4Q_o^2) + \sum_{r=1}^{\infty} \gamma_{2r} \cos 2rx\right] z = 0. \qquad 38$$

If all the γ terms except that for r = 1 are zero, Eq. 38 takes on the form of the well known Mathieu equation. The Mathieu equation is of greatest interest in parametron analysis although Hill's equation is of a

more general nature.

Equations of both the Hill and Mathieu types have been extensively investigated and reported by many writers (42-47). Of greatest interest in the parametron investigation is the question of stability. For certain values of parameters, solutions of the Hill and Mathieu equations exist which are stable, i.e., they are steady state solutions while for other values of parameters, the solutions are unstable and either increase without limit or decay to zero. In terms of the parameters of Eq. 38, these regions of stability and instability for the Mathieu equation are shown in Fig. 7(A) as the shaded and unshaded regions respectively.

Although the shaded regions of Fig. 7(A) represents a region of constant amplitude of oscillations for z, it represents a region in which any small disturbance of y decays with time because of the exponential term in Eq. 37 relating y and z. If a system with damping is to oscillate and have a nonzero output, then the damping, the tuning and the pump amplitude must be such that the system operating point lies somewhere in unshaded region of Fig. 7(A); the allowable areas yet to be determined.

Most references to the Hill's equation write it in the form

$$z'' + (\theta_o + 2 \sum_{r=1}^{\infty} \theta_{2r} \cos 2rx)\, z = 0. \qquad 39$$

The relation between the parameters of Eqs. 38 and 39 can easily be seen. The form of the solution of Eq. 39 has been taken by Whittaker and Watson (42) and by McLachlan (43, 44) as

$$z = \exp(\mu x) \sum_{r=-\infty}^{\infty} B_{2r} \exp(j2rx) \qquad 40$$

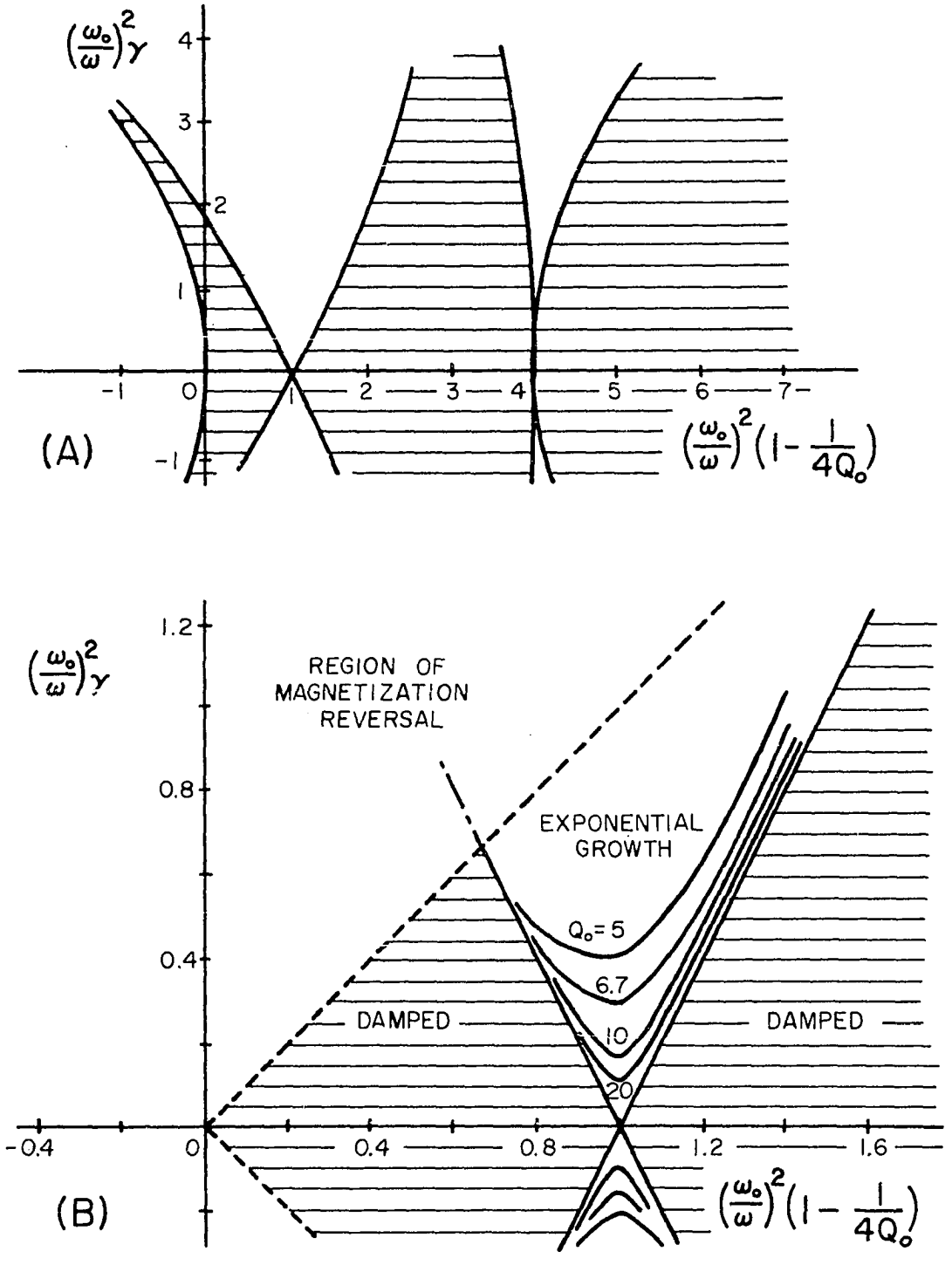

Fig. 7. (A) The stability regions of the Mathieu equation

(B) The stability regions of a "linearized" parametron for very low initial excitation levels

where $j = \sqrt{-1}$ and μ is a constant which may be real, imaginary or complex. Upon substituting Eq. 40 into Eq. 39 and equating like terms in powers of x, McLachlan (43) gives, provided $\theta \neq (2r)^2$, the relation

$$\sin^2(j\mu\pi/2) = \triangle(0)\, \sin^2(\pi\sqrt{\theta_o}/2) \qquad 41$$

where $\triangle(0)$ is an infinite determinant which for the Mathieu case can be written

$$\triangle(0) = \begin{vmatrix} \cdots & \cdots & \cdots & \cdots & \cdots & \cdots & \cdots \\ \cdots & 1 & \theta_2/(\theta_o-16) & 0 & 0 & 0 & \cdots \\ \cdots & \theta_2/(\theta_o-4) & 1 & \theta_2/(\theta_o-4) & 0 & 0 & \cdots \\ \cdots & 0 & \theta_2/\theta_o & 1 & \theta_2/\theta_o & 0 & \cdots \\ \cdots & 0 & 0 & \theta_2/(\theta_o-4) & 1 & \theta_2/(\theta_o-4) & \cdots \\ \cdots & 0 & 0 & 0 & \theta_2/(\theta_o-16) & 1 & \cdots \\ \cdots & \cdots & \cdots & \cdots & \cdots & \cdots & \cdots \end{vmatrix} \qquad 42$$

Of greatest interest in the case of the parametron are the Mathieu equation solutions in the large V-shaped region of Fig. 7(A) near unity on the abscissa. In this region the parametron circuit is resonant at approximately one-half the pump frequency, viz., $\omega_o \simeq \omega$ since $\omega_p = 2\omega$. For the case of the Mathieu equation, McLachlan (44) gives for the stable regions of Fig. 7(A) the two independent solutions

$$z_{1s} = \sum_{r=-\infty}^{\infty} b_m \cos(m + \phi)x$$

$$z_{2s} = \sum_{r=-\infty}^{\infty} b_m \sin(m + \phi)x \qquad 43$$

where b_m and ϕ are real constants dependent upon θ_o and θ_2. In the first stable region $m = 2r$ and in the second stable region $m = 2r + 1$.

For the unstable region of Fig. 7(A) between the first and the second stable regions, the solutions for the Mathieu equation are given by McLachlan as

$$z_{1u} = \exp(ax) \sum_{r=0}^{\infty} c_m \cos(mx + \varphi_m)$$

$$z_{2u} = \exp(-ax) \sum_{r=0}^{\infty} c_m \cos(mx - \varphi_m) \qquad 44$$

where in this region $m = 2r + 1$. In Eq. 44, c_m and φ are real constants dependent upon θ_o and θ_2 and a is a positive real number. From Eq. 44 one sees that one of the solutions of the Mathieu equation experiences an exponential growth. Thus one would expect that a physical system which obeyed the Mathieu equation would also have, under certain conditions, an exponential growth. A knowledge of the conditions under which this growth occurs and the rate of growth is of interest in the parametron case.

If one writes μ as the complex number $\sigma + j\beta$ where σ and β are real numbers, Eq. 41 for the case of the general Hill equation can be written in the form

$$\cosh \sigma\pi \cos \beta\pi + j \sinh \sigma\pi \sin \beta\pi = 1 - 2\Delta(0) \sin^2(\pi\sqrt{\theta_o}/2). \qquad 45$$

Equation 45 holds for all possible real values of θ_o and θ_{2r}. With the values of θ_{2r} restricted to having only real values, $\Delta(0)$ is also always real. A further restriction of θ_o to positive values is of interest here. One then concludes, since the right hand side of Eq. 45 is real, that

throughout the region of positive θ_o, either $\sinh \sigma\pi = 0$ or $\sin \beta\pi = 0$. The first case implies that $\sigma = 0$ so that $\cosh \sigma\pi = 1$. This condition requires the right hand side of Eq. 45 to have a value between +1 and -1. Thus, in the region where the right hand side of Eq. 45 has a value between +1 and -1, the μ of Eq. 40 is imaginary indicating that the solutions are stable and in the Mathieu case of the form of Eq. 43.

In the regions where $\sin \beta\pi = 0$, it is implied that $\beta = 0$ or ± 1 which in turn implies that $\cos \beta\pi = \pm 1$. If the right hand side of Eq. 45 has a magnitude greater than unity, one must choose the appropriate value of β to give the correct algebraic sign and determine the value of σ on the basis of magnitude. Since the cosh function is symmetric about $\sigma = 0$, the solutions for σ have two equal values, one positive and the other negative. These values of σ correspond to the values of "a" for the Mathieu solutions of Eq. 44. The dividing line between the stable and the unstable solutions of the Hill-Mathieu type of equations can be seen to occur when the right hand side of Eq. 45 has a magnitude of unity.

The stable regions for the Mathieu solutions have been extensively studied and tabulated, the most extensive tabulation being under the auspices of the U. S. National Bureau of Standards (46). In contrast, there is a dearth of available data on the unstable regions. McLachlan (43) in 1947 suggested that although none were available at that time, an extensive set of constant μ curves would be of great value in the applied fields. In a later publication, McLachlan (44) gives a relatively small sized figure showing a few iso - μ curves but no tables. Meixner and Schäfke (45) in 1954 refer to some 1943 calculations by Kotowski (47).

Kotowski's calculations are not very extensive and, when compared with those of the Bureau of Standards, appear to be slightly in error since his unstable regions overlap into the stable regions of the latter. Since it was felt that a set of curves similar to constant μ curves in the region $\theta_0 \simeq 1$ would be of value in parametron design studies, the infinite determinant of Eq. 42 was approximated by a 7 x 7 determinant and values of σ and β calculated on the I. S. U. Cyclone for a portion of this region. From these calculations the curves of Fig. 8 showing σ versus $\gamma = 2\theta_2 (\omega/\omega_0)^2$ for various values of $\theta_0 = (\omega_0/\omega)^2[1 - 1/4\ Q_0^2]$ were drawn.

In the immediately preceding discussion solutions of z have been considered. However, y is proportional to the quantity of actual interest, viz., the transverse flux linkage and its time rate of change. The quantities y and z are related by Eq. 37. Even though z may be unstable and tend to increase without limit with increasing x, y may actually decrease if the factor $(\omega_0/2\omega Q_0)$ in the exponential of Eq. 37 is larger than σ. The point where they are just equal is of considerable interest. For pumping magnitudes less than this critical value, no oscillations in y can ever start from zero initial conditions although it will be shown later that under certain conditions, once started by the presence of suitably large initial conditions, steady state oscillations can set in and be sustained.

Although there are many possible variants one could discuss relative to the parametron by considering the effect of independently varying ω, ω_0, γ or Q_0, the present discussion will be limited to the effect of varying ω and γ. This means that the parametron resonant circuit will be

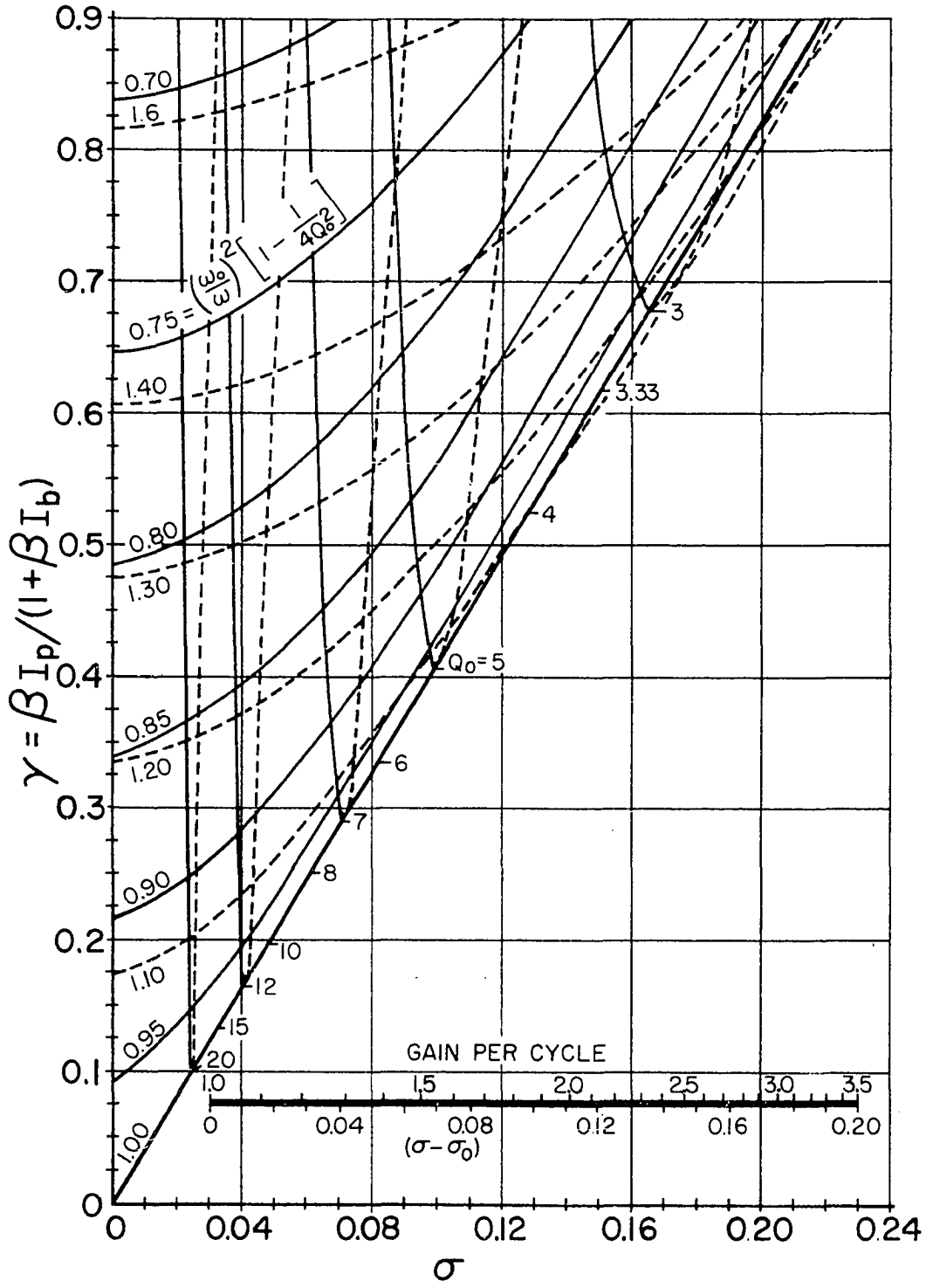

Fig. 8. A chart for the graphical determination of the stability and the initial gain per cycle of a "linearized" parametron

considered to remain fixed and only the frequency and amplitude of the pump changed. For a given value of ω_o/ω and of Q_o, one can determine a critical value of γ such that $\sigma - (\omega_o/2\omega Q_o) = 0$. Curves of constant Q_o are shown on Fig. 8.

A fixed parametron tank circuit will have a specific value for ω_o and Q_o. If a Q_o curve of the same value is picked on Fig. 8, then any choice of pump parameters ω and γ such that the operating point of the system lies on the right of this Q_o line will result in an unstable system and oscillations will start to build up from any small disturbance in the system. If one calls the σ of the operating point σ_o and the σ where the Q_o curve crosses the $(\omega_o/\omega)^2$ curve, $\bar{\sigma}_o$, then the growth will be at the exponential rate given as $\exp[(\sigma_o - \bar{\sigma}_o)x]$. If the operating point lies on the left of the Q_o curve, then any small disturbance will eventually damp out with an exponential rate given as $\exp[-(\sigma_o - \bar{\sigma}_o)x]$. Curves of constant Q_o are also shown on Fig. 7(B). An operating point chosen above the particular Q_o curve of interest results in a buildup of oscillations while a point below this contour results in a damping of oscillations.

It is important in any consideration of parametrons as computer elements to have some notion of the rate at which oscillation could be expected to build up. One simple way of expressing this is to state the gain per cycle, i.e., to state the ratio of the envelope amplitude at the end of a cycle to that at the beginning. Since the period of this oscillation is 2π, the gain per cycle is $\exp[2\pi(\sigma_o - \bar{\sigma}_o)]$. A scale relating gain per cycle to $(\sigma_o - \bar{\sigma}_o)$ is shown in Fig. 8. This permits an easy and rapid determination of gain per cycle to be made.

Although it must be realized that the Mathieu approximation of thin film parametron operation is good only at low amplitudes, it is nevertheless of considerable value in studying the conditions required to start oscillations and the initial rates of increase of such oscillations. As the amplitude increases more terms in Eq. 35 must be considered. The resultant equations do not lend themselves to easy analysis. With the I. S. U. Cyclone available it seemed advisable to attempt some numerical calculations on this problem for certain values of parameters and for certain initial conditions.

c. Some numerical solutions of the parametron equation As a first attempt at a numerical solution, parameters were picked so that Eq. 35 was approximated as

$$y'' + 0.1\, y' + 0.8\ [1 + \gamma \cos 2x][y + (1/2)y^3] = 0. \qquad 46$$

Computations were made for four different values of γ, viz., 0.5, 0.4, 0.3 and 0.25, and for two different initial conditions, viz., y(0) and y'(0) equal -0.2516 and 0.1634 respectively in one case and -0.3355 and 0.2719 respectively in the second case. It is to be noted that the initial condition values in the first case are three-fourths those of the second.

Figure 9(A) shows seven and one-half cycles of a y - y' plot of the solution for the case $\gamma = 0.5$ starting with the initial conditions y(0) = -0.2516 and y'(0) = 0.1634. It is to be noted that the magnitude of oscillation builds up more or less exponentially, overshoots somewhat and then drops back in an oscillatory manner toward an equilibrium amplitude.

Such y - y' plots are interesting and provide a very good picture of

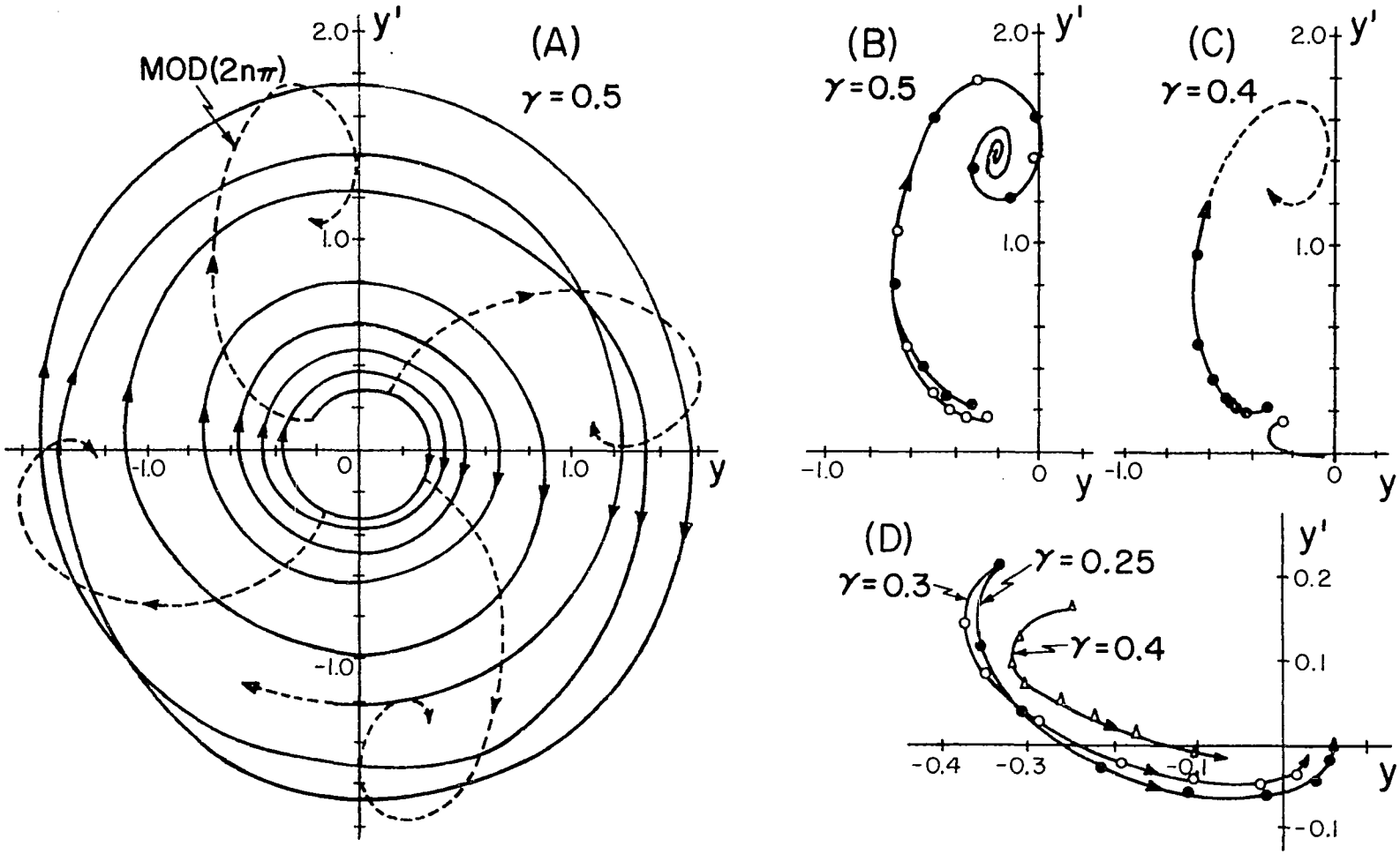

Fig. 9. Solution and modulus (2nπ) curves in the y - y' plane of the numerical solutions of the "linearized" parametron equation $y'' + 0.1\,y' + 0.8(1 + \gamma \cos 2x)(y + y^3/2) = 0$

what is happening as a function of time. However, they are difficult to plot and, in a case such as this where overshoot and a damped oscillation about an equilibrium final path occurs, they are difficult to follow once plotted. In addition, a good y - y' plot requires a substantial amount of computer time in just outputting sufficient results to make a good plot. In the case of periodic solutions where the y - y' plots during the growth period are known to approximate exponential spirals, it is more convenient to study the behavior of the solution at specific times relative to the pump cycle. These times can be designated as mod $(2n\pi)$, mod $(\pi/2 + 2n\pi)$, and so forth which simply means modulus $(\mathcal{T})$ = modulus $(2n\pi)$, etc. Four of these mod $(\mathcal{T})$ curves are shown in Fig. 9(A). It can be seen that a reasonable estimate of the y - y' plot can be obtained if one is given nothing more than one of these modulus curves.

Figures 9(B), 9(C) and 9(D) show mod $(2n\pi)$ solution curves for various values of γ in Eq. 46 and for the two sets of initial conditions. Figure 9(B) extends the mod $(2n\pi)$ curve of Fig. 9(A). It is to be noted, as one would expect, that after a few cycles the initial conditions no longer significally influence the solution. Although the solutions for different initial conditions do not have the same value at the same time relative to the pump waveform, they do follow along the same modulus curve. The spacing between the various dots and circles on the modulus curves of Fig. 9 indicate the time of one period of ω or two periods of the pump current. One can see from these modulus curves that the amplitude of the solution is very similar to the under damped response of an ordinary parallel RLC circuit to a unit step input.

It can be seen from Fig. 8 that for zero initial conditions, the Mathieu approximation has stable solutions for all values of γ cited above and that any small disturbance in the actual system would gradually damp out. However, Fig. 9(C) shows that depending upon the amplitude of the initial excitation, solutions of Eq. 46 either decay or build up. More will be mentioned on this "threshold excitation" later. Figure 9(D) shows three mod $(2n\pi)$ plots of damped solutions of Eq. 46.

The final rest values of the growing solutions of Fig. 9 are much in excess of unity. Since $y = 1$ is the maximum possible value of y, it is evident that neglecting powers of y greater than y^3 in Eq. 35 lead to substantial errors in determining the saturation amplitude. Subsequently the fifth power of y in Eq. 35 was added to the program. Numerical calculation on the equation

$$y'' + 0.1y' + 0.8\ [1 + 0.5 \cos 2x][y + (1/2)y^3 + (3/8)y^5] = 0 \qquad 47$$

was made. The mod $(2n\pi)$ for this solution is shown as (b) in Fig. 10. Addition of the fifth order term reduced the maximum value of the amplitude of y but y was still in excess of unity.

The next step was to modify the program to include the square root in Eq. 33 without the necessity of expanding as in Eq. 34. Numerical calculations were made on the equation

$$y'' + 0.1y' + 0.8\ \frac{1 + 0.5 \cos 2x}{\sqrt{1 - y^2}}\ y = 0. \qquad 48$$

A mod $(2n\pi)$ curve for this solution is shown as (c) in Fig. 10. This solution also exceeds the limit $y' = 1$ somewhat during overshoot but not

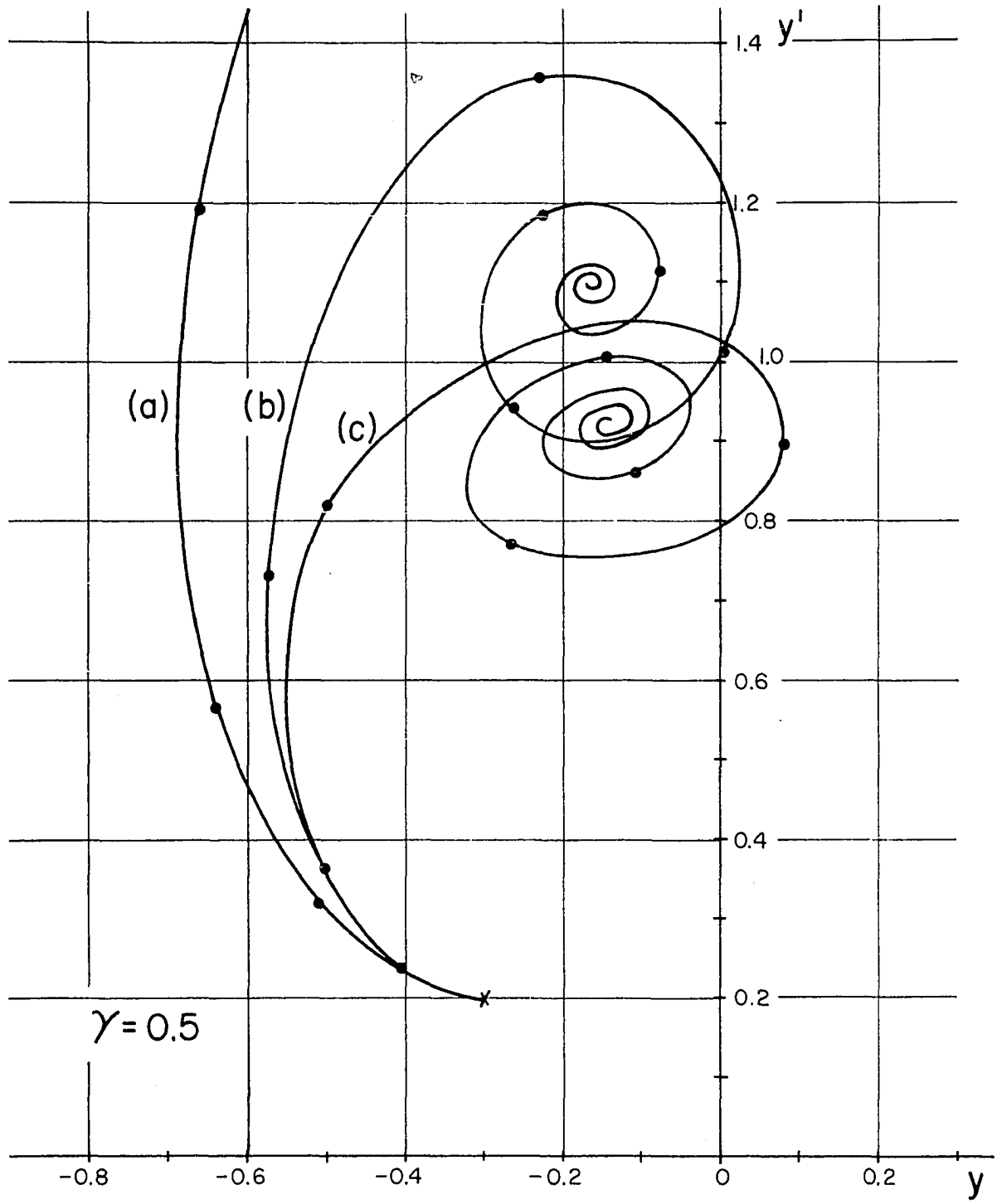

Fig. 10. Modulus ($2n\pi$) curves comparing the numerical solutions (a), (b) and (c) of the approximations of the "linearized" parametron as given by Eqs. 46, 47 and 48

nearly to the same extent as the previous solutions. For comparison purposes, the first portion of the solution for Eq. 46 for the same initial conditions is shown as (a).

The fact that the peak amplitude of the solutions for y in all the foregoing proposed parametron equations approach or exceed the value unity, invalidates the assumption made early in this discussion to the effect that the maximum angle of rotation of the magnetization vector should remain considerably less than 90 degrees. In an attempt to find a parametron equation which might more nearly describe the actual device, the idea of a "linearized" parametron equation was dropped and reference made to the model of a thin film inductor depicted in Fig. 4. If one again assumes that the air inductance L_o is small and can be absorbed into an effective value of capacitance C and conductance G in parallel with the nonlinear elements of Fig. 4, he can obtain an equation in y of the form

$$y'' + \frac{1 - y^2 + G_o/G}{1 - y^2 + C_o/C}\frac{\omega_o}{\omega Q_o}y' + \frac{C_o}{C}\frac{y(y')^2}{(1 - y^2)(1 - y^2 + C_o/C)} + \left[\frac{C + C_o}{C}\right] + \left(\frac{\omega_o}{\omega}\right)^2\left[\frac{1}{1 + \beta I_b} + \frac{\Gamma + \gamma \cos 2x}{(1 - y^2)^{1/2}}\right]\frac{y(1 - y^2)}{1 - y^2 + C_o/C} = 0 \qquad 49$$

where ω_o is the low level resonant angular frequency of the parametron tank circuit and where the other parameters have the same meaning as in the previous discussion. One might call this the "dynamic model" parametron. It should be noted that the discussion following Eq. 33 concerning the various solutions Y(x) applies equally well to Eq. 49.

The computer program was again modified to handle Eq. 49. The large

number of parameters in Eq. 49 makes any general discussion of the possible solutions very difficult. It was decided too limit the study to solutions for which $G_o/G = C_o/C = 0.1$. Figure 11 shows the growth characteristic of the solution of a highly biased parametron for the case $(1 + C_o/C)(\omega_o/\omega)^2 = (\omega_o'/\omega)^2 = 1$, $\Gamma = 1$, $\gamma = 0.4$, $Q_o = 9.55$ and $I_b = \infty$. According to Fig. 8, this equation should grow from zero initial conditions with a gain per cycle of about 1.23. A y - y' plane plot of this solution is shown in Fig. 11(A). Since during the growth period the path was an exponential spiral, one can see that a fairly good indication of the growth rate of the solution can be obtained by plotting the radial distance from the origin to the various points on the mod $(2n\pi)$ curve corresponding to integer values of n. Such a plot is shown in Fig. 11(B) both on a linear and on a logarithmic scale. The logarithmic scale indicates that the solution not only has an exponential growth as expected but that this exponential growth continues into the overshoot region. Measurements from Fig. 11(B) indicate the gain per cycle for amplitudes of this magnitude to be about 1.26. This is in good agreement with the 1.23 predicted by the Mathieu approximation.

A rerun of this problem starting with an initial condition of $y(0) = -0.0001$ and $y'(0) = 0.0001$ gave a gain of 1.21 per cycle in the very low amplitude regions. The choice of $C_o/C = 0.1$ is probably quite large and that in practice, a much smaller ratio would be observed.

For a pump parameter γ of 0.4, this circuit requires no threshold excitation but will build up from zero initial conditions. Reference to Fig. 8, however, indicates that if $(\omega_o'/\omega)^2$ were to be changed from 1.0 to

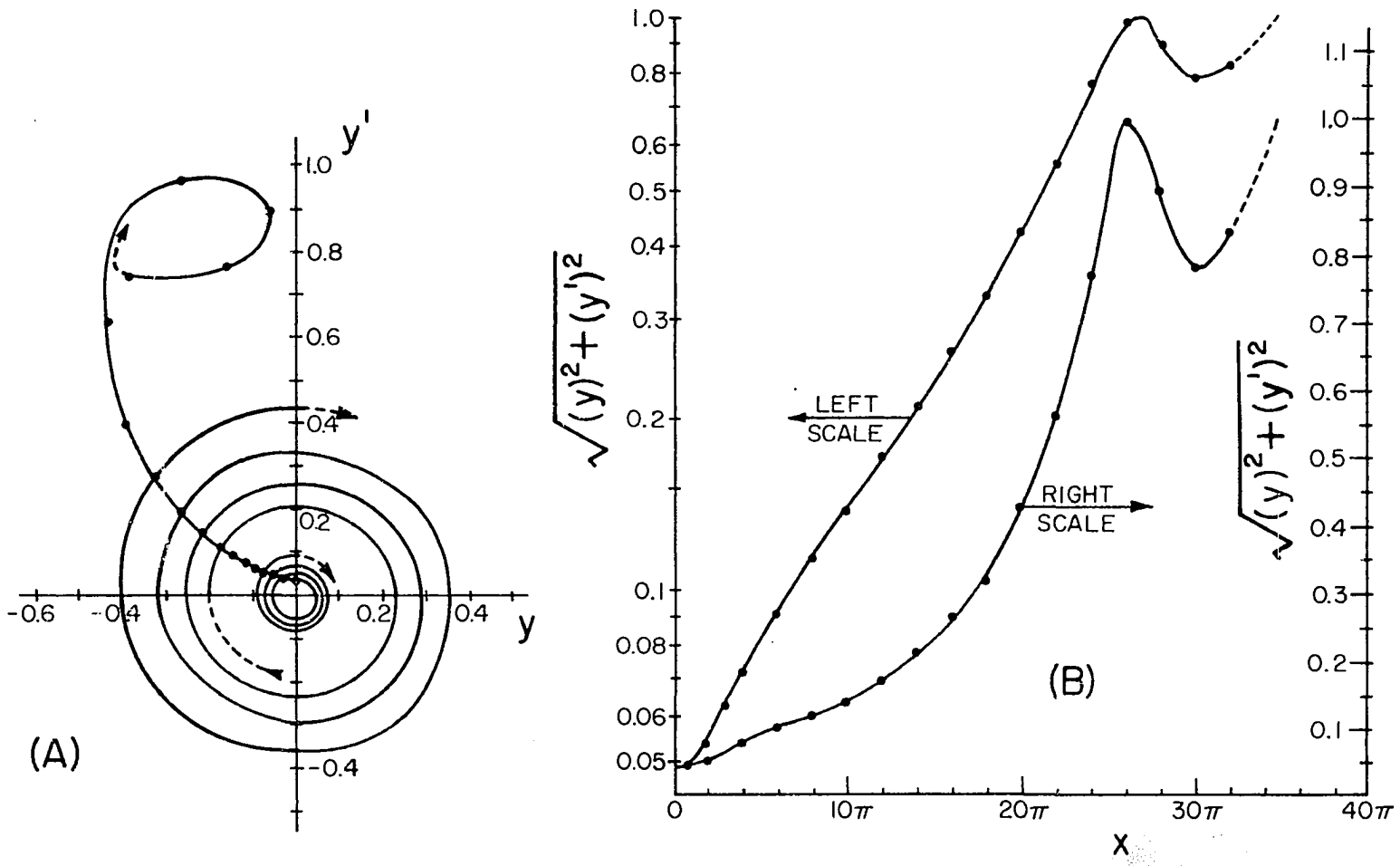

Fig. 11. The growth characteristic of a highly biased "dynamic model" parametron obeying the equation

$$y'' + 0.1y' + 0.1y(y')^2/(1 - y^2)(1.1 - y^2) + (1 + 0.4 \cos 2x)y(1 - y^2)^{1/2}/(1.1 - y^2) = 0$$

0.8, the system would not build up oscillations from zero initial conditions. In order to investigate the threshold conditions in such a case numerous computer calculations were made for a highly biased parametron with the parameters of Eq. 49 having values of $(\omega_o'/\omega)^2 = 0.8$, $I_b = \infty$, $\Gamma = 1$ and γ having values of 0.25, 0.3, 0.35, 0.4 and 0.5. A portion of these results are shown in Fig. 12. The set of mod $(2n\pi)$ curves of Fig. 12(A) show quite clearly the presence of a threshold excitation level for the case $\gamma = 0.4$. A similar curve for $\gamma = 0.25$ is shown in Fig. 12(B). From a number of y - y' plots such as those of Figs. 12(A) and 12(B) one can make a y - y' plot of the excitation threshold for various values of γ as illustrated in Fig. 12(C).

The numerical calculations were allowed to proceed until a final steady state amplitude was reached. This amplitude was found to be very near unity in value. A y - y' plane plot for a complete cycle of steady state parametron oscillation was calculated for this final value of amplitude. This is shown as the large nearly circular heavily lined curve of Fig. 12(A). Flanking this curve are two true circles for comparison. The fact that this is nearly circular indicates that the oscillation waveform of a highly biased parametron should have a very low harmonic content if Eq. 49 is a reasonably good mathematical representation of it.

Attention should be called to the fact that the modulus curves of Fig. 12 are exactly duplicated by another set in the lower half of the y - y' plane. This second set can be obtained by simply rotating the first set 180 degrees around the origin. In view of a previous discussion following Eq. 33 concerning a reversal of the bias, it can be seen that bias reversal

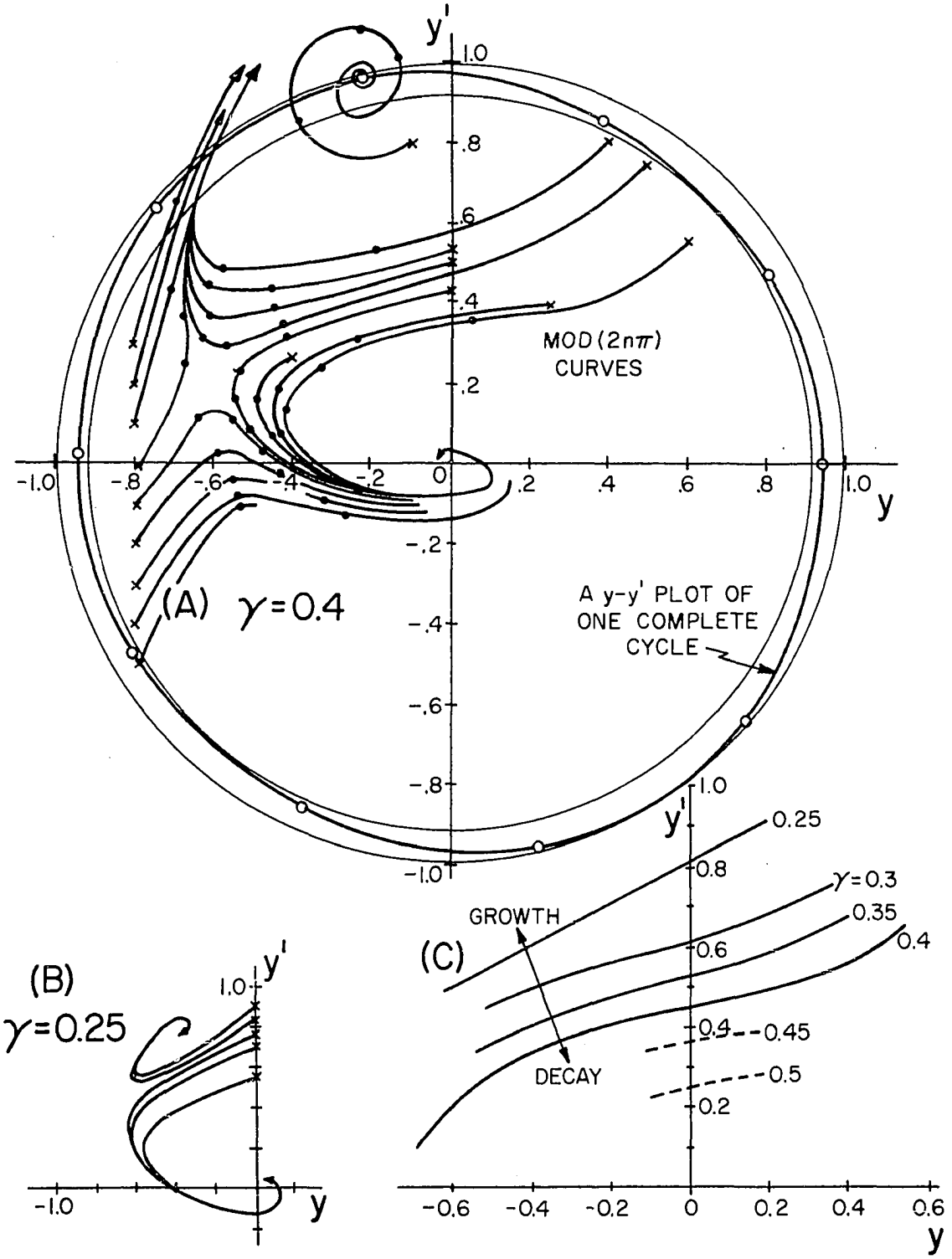

Fig. 12. A study of the threshold characteristics of a highly biased "dynamic model" parametron obeying the equation $y'' + 0.1y' + 0.1y(y')^2/(1-y^2)(1.1-y^2) + 0.8(1+\gamma\cos 2x)y(1-y^2)^{1/2}/(1.1-y^2) = 0$

will result in two more sets of modulus curves identical to the two above but rotated about the origin 90 degrees from them.

The requirement that excitation must exceed a certain threshold before self-sustaining oscillations set in and the fact that two different stable oscillation phase states of the same amplitude but differing in phase by 180 degrees leads one to predict the possibility of a three state device, i.e., a device with a stable (+) state, a stable zero state and a stable (-) state. If bias reversal is permitted, a five state device is predicted.

The preceding analysis barely touches the surface of the possible calculations that can be made. Future calculations are planned in which a study will be made of the effects some of the other parameters in the equation have on the gain per cycle, the threshold excitation levels required to induce oscillations and upon the final steady state amplitude. Future studies are also planned in which an attempt will be made to experimentally check the validity of the equivalent circuit of the thin film inductor of Fig. 4 and the range over which it applies. Some additional terms may be required to take into account the nonhomogenous effects at large rotation angles that are known to exist but which have been omitted.

3. Experimental verification of the thin film parametron operation

To experimentally verify some of the results of the preceding analysis, a thin film parametron was constructed from a three millimeter square section of a 6000 angstrom thick 80-20 permalloy film deposited on a six mil thick glass substrate. This was wound with 35 turns of No. 40 copper wire to form the transverse winding of the parametron inductor. The

measured inductance of this winding was approximately 1.65 microhenry, approximately one-half of this inductance attributable to the film. A pump winding consisting of 52 turns of No. 40 wire with its centertap grounded was wound in a flat solenoid in such a manner that the transverse winding and film could be inserted mutually perpendicular to it in the manner indicated schematically in Fig. 1(B). The pump winding was driven in push-pull by two Fairchild 2N697 transistors which could be gated on and off by a square wave pulse from a Hewlett-Packard 211 Square Wave Generator. A Hewlett-Packard 150A Oscilloscope was used to display the parametron waveforms. Magnetic bias was supplied by a small horseshoe magnet placed approximately two inches from the film.

The parametron was observed to function at a pump frequency of about 25 megacycles per second. However, synchronizing problems with the equipment available proved quite difficult so that the pump frequency was lowered to 14.3 mc/s. The Q_0 of the parametron tank circuit was measured to be about 12. Figure 13(A) shows the gated 14.3 mc/s, 16.4 volt peak-to-peak pump voltage across one side of the pump winding. Figure 13(B) shows the exponential increase, the overshoot and finally the steady state level followed by the exponential decay of the 7.15 mc/s parametron tank voltage as the pump was gated on and off. Figure 13(C) shows on an expanded scale a portion of the exponential rise of Fig. 13(B) superimposed over the waveform of the pump. Measurements from Fig. 13(C) give a value of between 1.55 and 1.65 for the gain per cycle. It was found experimentally that the circuit would barely oscillate when the peak-to-peak pump voltage across one side of the pump winding was 5.5 volts, i.e., at

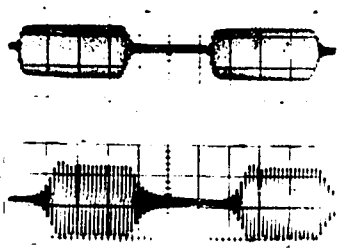

(A)

(B)

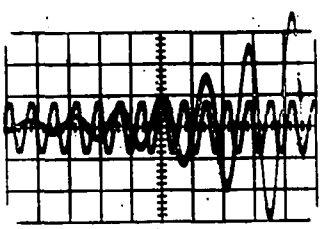

(C)

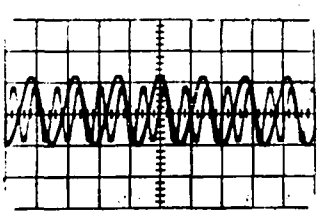

(D)

$$\frac{\omega}{2\pi} = \frac{\omega_o}{2\pi} = 7.15 \text{ mc/s}; \quad Q_o = 12$$

Fig. 13. The gain, saturation and decay characteristics of an experimental thin film parametron

one-third the value used for Fig. 13. With this information one can compare this experimental value with the initial gain per cycle expected on the basis of the Mathieu approximation. One first determines the difference in σ between the point where the $Q_o = 12$ curve touches the $(\omega_o/\omega)^2 = 1$ line to a point also on the $(\omega_o/\omega)^2 = 1$ line but for a γ three times as great from Fig. 8, i.e., one first determines $\sigma_o - \bar{\sigma}_o$, which in this case is about 0.080. On the conversion scale of Fig. 8 one finds a predicted gain per cycle of about 1.65, in reasonably good agreement with the experimental value.

Figure 13(D) shows the relative phase of the pump and oscillations at saturation. Whereas in Fig. 13(C) where oscillations are just beginning the peak of oscillation occurs at the same time as a peak in pump amplitude, it is easily seen in Fig. 13(D) that at saturation the oscillations lead the pump by approximately one-eighth of a cycle of oscillation.

When the frequency of the pump was raised from 14.3 to 15.6 mc/s but without any corresponding retuning of the parametron tank circuit, it was observed that it required a peak-to-peak voltage across one side of the pump winding of approximately 18 volts before oscillations would start. Once started, however, oscillations were sustained until the pump voltage dropped to approximately one-half this value. The parametron has a rather large hysteresis with respect to pump amplitude.

One would expect from Fig. 8 that changing the pump frequency would require a substantially greater pump amplitude for oscillations to start. Since for a Q_o of 12, it required 5.5 volts peak-to-peak for oscillations to start in a resonant parametron tank, one would predict from Fig. 8 that for a $(\omega_o/\omega)^2 = 0.84$, a voltage of

5.5 x (0.435/0.165) ≈ 14.5 volts peak-to-peak

would be required. This is in good agreement with the experimental results above when one considers that an increase in frequency results in a lowering of pump winding current for a given voltage. Assuming a pure inductance for the pump winding, a correction for this frequency gives a required voltage of

$14.5/(0.84)^{1/2}$ = 15.8 volts peak-to-peak.

To facilitate synchronizing the oscilloscope, measurements of various phase states were made with the parametron tank circuit resonant at $\omega_o/2\pi$ = 2.75 mc/s and at a constant pump amplitude. Figures 14(A) and 14(C) show the 5.5 mc/s pump voltage for the condition $\omega = \omega_o$. Figure 14(B) shows the two parametron states $\pm Y(\omega t)$ discussed earlier following Eq. 33. Reversing the bias, in this case by simply rotating the small horseshoe bias magnet, results in the two parametron states shown in Fig. 14(D). It is evident that these latter two states correspond to the states $\pm Y(\omega t + \pi/2)$ that were also discussed following Eq. 33. Thus, for a given pump amplitude and phase, a parametron oscillating at resonance has four possible stable modes.

The frequency of the pump was then increased to 6.1 mc/s. Figures 14(E) and 14(G) show the pump in this case. The amplitude of the pump and the tuning of the parametron tank were not changed. Here the "threshold" character of the parametron is quite well demonstrated. The straight line of Fig. 14(F) indicates the stable zero output state. When the amplitude of a signal induced into the parametron tank exceeded a certain critical value, oscillations started which built up into either the (+) or the (-)

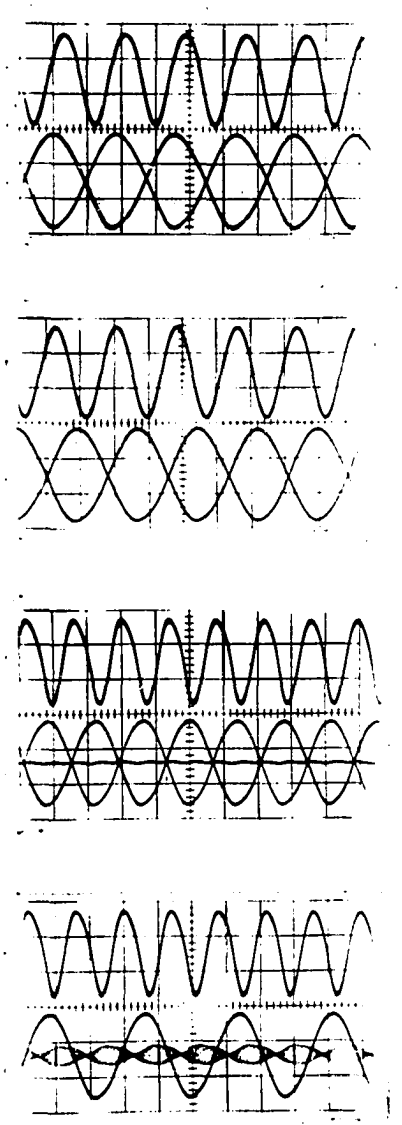

Fig. 14. Oscillograms illustrating the steady-state outputs of an experimental thin film parametron

phase of Fig. 14(F). Figure 14(H) gives an indication of the threshold amplitude required to trigger the parametron into oscillation. When a signal slightly different in frequency from one-half the pump frequency is coupled into a nonoscillating parametron tank, parametric amplification occurs. This amplification, however, is very phase sensitive. This gives rise to the beat note waveform of Fig. 14(H). When the incoming signal exceeded the amount shown, oscillations set in and the parametron output increased rapidly to the saturation amplitude shown. Here again, reversing the bias gives two additional stable phase states displaced 90 degrees from the other two; five stable states in all if bias reversal is permitted.

The experimental results reported here are in a large measure due to Pohm. These experimental results along with others and a simpler but less accurate formulation of the parametron problem are currently being published elsewhere in an article in which this writer is one of four authors (48).

4. Summary comments on the thin film parametron

In the discussion thus far, some of the technical aspects of individual parametrons have been considered. The application of several parametrons in a circuit to perform a logic function has not been examined, such a topic being considered beyond the scope of this thesis. With a computer element of this type, one should be able to achieve a degree of logical flexibility not normally found in a simple computer element. Ways and means for utilizing these elements in logic circuits are currently being studied (50, 51).

There are a number of facets of the thin film parametron problem which as yet remain unexplored, particularly from an experimental viewpoint. One of these is the question of high frequency operation. An analysis of the problem of operating a parametron in the frequency range of 100 to 500 mc/s has been considered by Pohm with this writer and others as coauthors (49). Using an analysis somewhat more simplified than that used here, it was shown that operation in this frequency range should be feasible. Strip line construction techniques are proposed.

With 80-20 permalloy as the film material, operating frequencies in excess of 1000 mc/s appear doubtful. In order to keep the operating frequency below the electronic resonance frequency, relatively high bias fields are required. This then requires high pumping fields which place substantially higher power requirements on the pump source. Whereas the losses in the tank circuit of the parametron and in the material amounted to only about three milliwatts for seven mc/s operation, it is estimated that losses would be in the order of 10 to 20 milliwatts at 500 mc/s. A continuation of the work described here will include a study of the thin film parametron operation at these higher frequencies.

C. Thin Film Inductors as Parametric Amplifier Elements

In addition to parametron operation, which is in reality a degenerate type of parametric amplifier operating under oscillatory conditions, thin film inductors can be used as the nonlinear reactance elements in parametric amplifiers. In this section, some considerations of such an application to negative resistance, lumped constant parametric amplifier circuits will be given for the case where the maximum angle of rotation ϕ

of the magnetization vector $\vec{M}$ is small and where the maximum frequency of operation is low enough that the elements shunting the nonlinear inductance of Fig. 4 can be neglected.

1. Multiple component small transverse signal inputs

With a single frequency pumping field, assume the inductance of the transverse winding is given by Eq. 18, the quasi-static expression for inductance under the assumption of small angles of rotation. Consider the somewhat restricted case where the only transverse magnetic fields in the film arise from currents flowing in the transverse winding itself rather than in a parallel winding. Further, suppose that this current contains many different frequency components, not necessarily harmonically related such that the current can be expressed as

$$i_T = \sum_{m=0}^{\infty} I_m \sin(\omega_m t + \theta_m). \qquad 50$$

The flux linkage in the transverse winding is then found by taking the product of Eq. 18 and Eq. 50 to give

$$\lambda_T = L_o\left[(1 + a_o/2) + \sum_{n=1}^{\infty}(-1)^n a_n \cos n\omega_p t\right]\left[\sum_{m=0}^{\infty} I_m \sin(\omega_m t + \theta_m)\right]$$

$$= L_o(1 + a_o/2)\sum_{m=0}^{\infty} I_m \sin(\omega_m t + \theta_m)$$

$$+ L_o \sum_{n=1}^{\infty}\sum_{m=0}^{\infty}(-1)^n a_n I_m \cos n\omega_p t \sin(\omega_m t + \theta_m). \qquad 51$$

The latter terms of Eq. 51 can be written as

$$L_o \sum_{n=1}^{\infty} \sum_{m=0}^{\infty} (-1)^n a_n (I_m/2) \left[\sin[(n\omega_p+\omega_m)t+\theta_m] - \sin[(n\omega_p-\omega_m)t-\theta_m] \right] .$$

Substituting this into Eq. 51 and then taking the first derivative with respect to time gives the induced voltage in the transverse winding as

$$\begin{aligned} e_T = {} & + L_o(1 + a_o/2) \sum_{m=1}^{\infty} I_m\omega_m \cos(\omega_m t + \theta_m) \\ & + L_o \sum_{n=1}^{\infty} \sum_{m=0}^{\infty} (-1)^n a_n I_m/2 \left[(n\omega_p+\omega_m) \cos[(n\omega_p+\omega_m)t+\theta_m] \right. \\ & \left. - (n\omega_p-\omega_m) \cos[(n\omega_p-\omega_m)t-\theta_m] \right] . \end{aligned} \qquad 52$$

Suppose that one now considers the power input to the transverse winding by each of the current components of Eq. 50 taken individually. In doing this consider the winding resistance to be external to the winding itself. Call the current component of interest i_s where $i_s = I_s \sin(\omega_s + \theta_s)$. The instantaneous power input to the transverse winding due to this current is $p_{in-s} = i_s e_T$ where e_T is given by Eq. 52. Taking this product and expanding by trigonometric identities gives

$$\begin{aligned} p_{in-s} = {} & L_o(1 + a_o/2) \sum_{m=1}^{\infty} \omega_m (I_s I_m/2) \left[\pm \sin[(\omega_m \pm \omega_s)t + \theta_m \pm \theta_s] \right] \\ & + L_o \sum_{n=1}^{\infty} \sum_{m=0}^{\infty} (-1)^n a_n (I_s I_m/4) \left[\pm(n\omega_p + \omega_m) \sin \right. \\ & [(n\omega_p + \omega_m \pm \omega_s)t + \theta_m \pm \theta_s] \mp (n\omega_p - \omega_m) \sin \\ & \left. [(n\omega_p - \omega_m \pm \omega_s)t - \theta_m \pm \theta_s] \right] \end{aligned} \qquad 53$$

where the upper signs go together and where both the upper and the lower

signs must be included in the summation.

The average power input to the transverse winding supplied by the source of the current i_s can be found from Eq. 53 by use of the integral

$$P_{in-s} = \lim_{T \to \infty} (1/2\ T) \int_{-T}^{T} p_{in-s}\ dt. \qquad 54$$

It can readily be seen from Eq. 53 that the average power input to the transverse winding will be zero unless there are certain values of N and M where for n = N and n = M, a given s will meet at least one of the following six conditions:

(a) $\omega_M = \pm\omega_s$

(b) $\omega_M = \pm(N\omega_p + \omega_s)$

(c) $\omega_M = \pm(N\omega_p - \omega_s)$.

Since all frequencies are assumed to be positive real, the conditions given by the negative signs of (a) and (b) can never contribute to the average power input. In addition, unless $\omega_s \geq N\omega_p$ the negative sign of (c) can not contribute. Likewise unless $\omega_s \leq N\omega_p$, the positive sign of (c) does not contribute to the average power. If i_s is the total current at the angular frequency ω_s flowing in the transverse winding, one has for condition (a) that $M \equiv s$. In such a case $\theta_M \equiv \theta_s$ and hence the first term of Eq. 53 contributes nothing to the average power. Under certain conditions, however, all the current at $\omega_M = \omega_s$ may not be a direct result of the current i_s from the source. In this case one must consider whether or not $M \equiv s$ whenever the condition $\omega_M = \omega_s$ arises. There now are three other conditions to consider, viz.,

(b') $\omega_M = N\omega_p + \omega_s$

(c') $\omega_M = N\omega_p - \omega_s$

(c") $\omega_M = \omega_s - N\omega_p$.

A general consideration of all the facets of these conditions is well beyond the scope of this thesis. However, if the subscript s is taken to indicate an externally supplied signal, then three cases are of practical interest, viz.,

(i) $\omega_M = N\omega_p + \omega_s$ and $\omega_{M'} = N\omega_p - \omega_s$ when $\omega_s \ll N\omega_p$

(ii) $\omega_M = N\omega_p - \omega_s$ when $\omega_s \cong N\omega_p$ and/or

$\omega_M = -N\omega_p + \omega_{s'}$ when $\omega_{s'} \cong N\omega_p$

(iii) $\omega_M = N\omega_p - \omega_s$ when $\omega_s < N\omega_p$.

Cases (i) and (ii) indicate the possibility of using thin film inductors as suppressed carrier balanced modulators and demodulators respectively. A discussion of the first of these possibilities will be postponed until later and a discussion of the second will not be attempted. The relationships in (iii) are the same as those given by Rowe and Manley (35, 36) for the case of nonlinear reactance parametric amplifiers. A consideration of the amplifier possibilities follows next.

2. The thin film inductor in a parametric amplifier

It is customary in analyzing parametric amplifiers to assume that the tuned circuits in the system prevent current flow from all but a very few of the great many harmonic and interproduct voltages induced by the action of the nonlinear element. This assumption is made in the interest of simplicity and ease of analysis. Here also in the interest of simplicity,

it will be assumed that the circuit elements external to the thin film inductor so restrict the flow of current that only the two currents i_1 and i_2 of Eq. 50 which have the frequency relationship $\omega_1 + \omega_2 = N\omega_p$ can flow in the transverse winding, all other currents at other frequencies being negligible. Using Eq. 54 to evaluate the time average of Eq. 53 for this condition and noting that $\omega_1 = N\omega_p - \omega_2$ and that $\omega_2 = N\omega_p - \omega_1$, one has

$$P_{in-1} = (-1)^{N+1} a_N L_o (I_1 I_2/4)\omega_1 \sin(\theta_1 + \theta_2) \qquad 55$$

and

$$P_{in-2} = (-1)^{N+1} a_N L_o (I_1 I_2/4)\omega_2 \sin(\theta_1 + \theta_2). \qquad 56$$

It is also customary in circuit theory to associate a resistance with the concept of power. Therefore assume that the resistive component of the input impedance to the inductor at ω_1 is R_{in-1} and at ω_2 is R_{in-2}. The respective powers at these frequencies can be expressed as $P_{in-1} = (1/2)I_1^2 R_{in-1}$ and $P_{in-2} = (1/2)I_2^2 R_{in-2}$. When these are equated with Eqs. 55 and 56 one has an expression for the input resistance as

$$R_{in-1} = (1/2)(I_2/I_1)(-1)^{N+1}\omega_1 a_N L_o \sin(\theta_1 + \theta_2) \qquad 57$$

and

$$R_{in-2} = (1/2)(I_1/I_2)(-1)^{N+1}\omega_2 a_N L_o \sin(\theta_1 + \theta_2). \qquad 58$$

In terms of the simplified system with only two currents permitted to flow in the inductor, and subject to the condition that $\omega_1 + \omega_2 = N\omega_p$, one can re-examine Eq. 52. Equation 52 can be reduced in complexity by this simplification and then upon performing a trigonometric expansion and the collecting of similar terms one has

$$e_T = I_1\cos(\omega_1 t+\theta_1)(\omega_1 L_o)[(1+a_o/2)-(-1)^N a_N(I_2/2I_1)\cos(\theta_1+\theta_2)]$$
$$+ I_1\sin(\omega_1 t+\theta_1)(\omega_1 L_o)[(-1)^{N+1}a_N(I_2/2I_1)\sin(\theta_1+\theta_2)]$$
$$+ I_2\cos(\omega_2 t+\theta_2)(\omega_2 L_o)[(1+a_o/2)-(-1)^N a_N(I_1/2I_2)\cos(\theta_1+\theta_2)]$$
$$+ I_2\sin(\omega_2 t+\theta_2)(\omega_2 L_o)[(-1)^{N+1}a_N(I_1/2I_2)\sin(\theta_1+\theta_2)]$$
$$+ \text{higher frequency terms.} \qquad 59$$

Comparing Eq. 59 with Eqs. 57 and 58 one notes that the coefficient of the transverse winding voltage components in phase with the input currents i_1 and i_2 is simply what was identified in the earlier equations as the resistive component of the input impedance of the transverse winding. The coefficient of the components of transverse winding voltage that is 90 degrees out of phase with the input currents can then be identified as the reactive components of the input impedance, the higher frequency terms being neglected. The reactive components of the input impedance of the transverse winding at the two angular frequencies ω_1 and ω_2 are then

$$X_{in-1} = \omega_1 L_o[(1 + a_o/2) - (1/2)(I_2/I_1)(-1)^N a_N \cos(\theta_1 + \theta_2)] \qquad 60$$

and

$$X_{in-2} = \omega_2 L_o[(1 + a_o/2) - (1/2)(I_1/I_2)(-1)^N a_N \cos(\theta_1 + \theta_2)]. \qquad 61$$

Suppose the transverse winding is now connected into a circuit such that looking back into the circuit from the terminals of the transverse winding one sees at an angular frequency of ω_1 a resistance R_1 and a reactance which is the negative of Eq. 60 and at ω_2 a resistance of R_2 and a

reactance which is the negative of Eq. 61. The total impedance around the system to the current i_1 flowing in the transverse winding will be a resistance $R_I = R_1 + R_{in-1}$ and to the current i_2 a resistance $R_{II} = R_2 + R_{in-2}$. If an equivalent voltage source e_1 at an angular frequency of ω_1 causes the current $i_1 = I_1 \sin(\omega_1 t + \theta_1)$ to flow in circuit I including the transverse winding, and if the only voltage source in circuit II is stray pickup and thermal noise so that the magnitude of any i_2 is very small, it will be noted that R_I will essentially be equal to R_1 and that R_{in-2} will be very much larger than R_2 provided $\sin(\theta_1 + \theta_2) \neq 0$. It is not difficult to visualize that there will be momentary transient currents in circuit II which will have at some instant the proper phase θ_2 to make $(-1)^{N+1} \sin(\theta_1 + \theta_2)$ negative, thus making R_{II} negative and causing the momentary current i_2 to increase. Since R_{in-1} has the same sign as R_{in-2}, R_I will then decrease allowing i_1 to increase, which in turn increases i_2, and so forth until an equilibrium point is reached where $R_2 + R_{in-2} = 0$ and $i_2 = I_2 \sin(\omega_2 t + \theta_2)$, $\omega_2 = N\omega_p - \omega_1$. During this build up process, the phase angles θ_1 and θ_2 may shift somewhat from their initial values as a result of detuning changes occurring as the reactance and resistance in the circuit change. In the terminology of parametric amplifier practice, circuit I above is called the signal circuit and circuit II the idler circuit.

Since $R_2 + R_{in-2} = 0$, one can solve for the terms common to both R_1 and R_{II} and obtain at equilibrium

$$(I_2/I_1)(R_2/\omega_2) = (1/2)(-1)^N a_N L_o \sin(\theta_1 + \theta_2). \qquad 62$$

Substituting Eq. 62 into the expression for R_I gives

$$R_I = R_1 - (I_2/I_1)^2 (f_1/f_2) R_2. \qquad 63$$

From Eq. 62 one can see that since the inductance coefficient a_N increases with increasing pump current, the ratio (I_2/I_1) will likewise increase as the pump current increases. Equation 63 then shows that the total resistance in circuit I will decrease as pump current increases. This decrease in the resistance of circuit I will give rise to an increase in I_1. For a given increase in pump current, the exact magnitude of this increase will be very dependent upon just how well the reactance elements in circuit I are tuned out.

If one is interested in amplification at the signal frequency $f_1 = \omega_1/2\pi$ and if it is assumed that the useful load makes up the majority of the resistance R_1, then a measure of the power gain at f_1 can be made by calculating the $I_1^2 R_1$ values with and without the pump on. A simple algebraic computation gives the ratio of power with pump to power without pump as

$$\text{relative signal power gain} = \frac{1}{\left[1 - \dfrac{I_2^2 R_2/f_2}{I_1^2 R_1/f_1}\right]^2}. \qquad 64$$

If instead the system is to act as a frequency converter and if the resistance R_2 is the load, then a measure of the conversion gain of the system is the ratio of the output power at the idler frequency $f_2 = \omega_2/2\pi$ to the signal power input at f_1. Again a simple computation gives this gain as

$$\text{relative converter power gain} = \frac{f_2/f_1}{\left[\dfrac{I_1^2 R_1/f_1}{I_2^2 R_2/f_2} - 1\right]}. \qquad 65$$

Equations 64 and 65 do not appear to be of any great value in computing power gains in a practical situation because of the difficulties in determining the ratio of the two currents. These equations do show, however, that both power gains increase without limit as the energy lost during a cycle of the signal frequency approaches the energy lost during a cycle of the idler frequency. When this point is reached where the two losses are equal, the system will have infinite power gain, and be capable of sustained outputs without inputs. At this point the system will break into oscillation, simultaneously oscillating at both frequencies f_1 and f_2, where conditions still require that $\omega_1 + \omega_2 = N\omega_p$.

3. Experimental verification of the thin film parametric amplifier

The analytical developments of the preceding paragraphs indicate the potential usefulness of inductors made of thin ferromagnetic films in parametric amplifier circuits. Some exploratory investigations were therefore made in which a 6000 angstrom permalloy film was used as the nonlinear element.

In order to instrument a simple experimental system with equipment readily available, a pump frequency in the range of 24 to 28 mc/s and signal frequencies in the range of 8 to 12 mc/s were chosen. Investigation in this frequency range permitted direct viewing of the r.f. output voltage on a Hewlett-Packard 150A Oscilloscope without the necessity of any intervening demodulation devices.

Figure 15 is a schematic diagram of the circuit used in most of the investigation described in this section. The transistor oscillator was adjustable over a range of 20 to 30 mc/s. Its r.f. output was controlled by

Fig. 15. The schematic diagram of the exploratory parametric amplifier used in this study

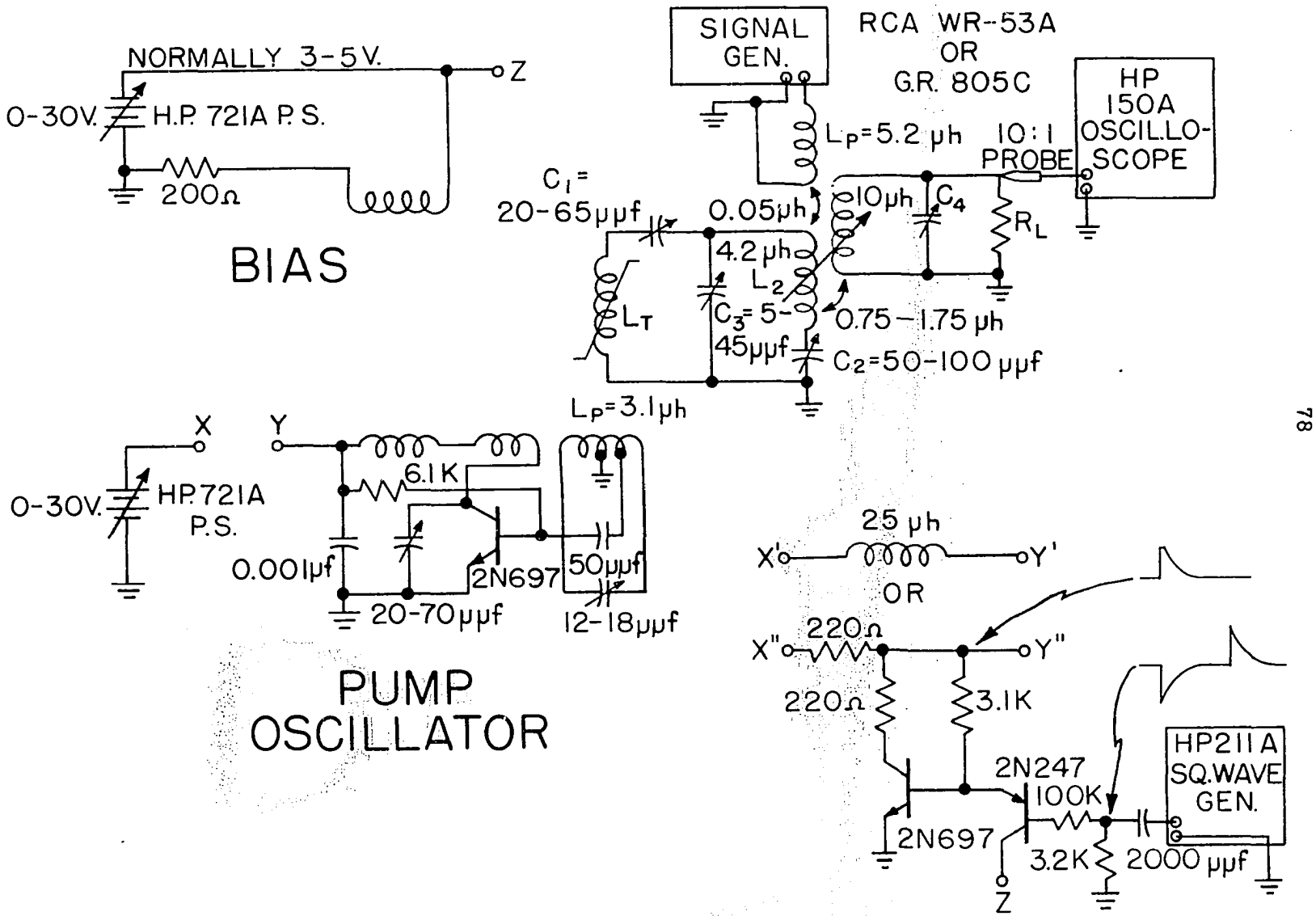
NORMALLY 3-5V.
Z
0-30V.
H.P. 721A P.S.
200Ω
BIAS
SIGNAL GEN.
RCA WR-53A
OR
G.R. 805C
HP 150A OSCIL.LO-SCOPE
10:1 PROBE
L_P=5.2 μh
C_1=
20-65μμf
0.05μh
10μh
C_4
R_L
4.2μh
L_2
L_T
C_3= 5-45μμf
0.75-1.75 μh
C_2=50-100 μμf
L_P=3.1μh
X
Y
0-30V.
HP.721A P.S.
6.1K
0.001μf
2N697
50μμf
20-70μμf
12-18μμf
PUMP OSCILLATOR
25 μh
X'
Y'
OR
X"
220Ω
Y"
220Ω
3.1K
2N247
100K
2N697
3.2K
2000 μμf
HP211A SQ.WAVE GEN.
Z

adjusting the d.c. power supply voltage either manually or by the shunting pulse circuit shown as x" - y". Physically the signal winding consisted of about 40 turns of No. 40 enamel wire wound around the permalloy film-glass substrate core as depicted in Fig. 1(B) to give a rectangular coil having inside dimensions of 1/4 by 1/4 by 6/1000 inches. The pump winding was wound with some 30 turns of No. 28 enamel wire to form a rectangular coil having a cross section of 5/8 by 1/10 inches and a length of 1/4 inch. The signal winding slipped into the center of the pump winding and was adjusted to be mutually perpendicular to it. The arrangement here was almost identical except for physical size to that used in the parametron studies. The bias winding was wound parallel to the pump winding on a form which served to keep the two windings separated by at least one-fourth inch. This separation kept the stray capacitance of the pump winding near a minimum. Figure 2, as previously mentioned, shows the signal winding inductance of this arrangement as a function of a d.c. bias current I_B in the bias winding or of a d.c. current I_b in the pump winding.

Figure 16 is an actual frequency response curve of the system of Fig. 15 as the input frequency is swept over a range. The different traces correspond to different pump powers and to different loads. The center of the sweep in each case is 9.5 mc/s with a sweep scale of 50 kc/s per division. Data obtained from this photograph and from data recorded at the time it was taken were used to plot Fig. 17. The lettered points on Fig. 17 correspond to data from the various traces of Fig. 16.

Some rough measurements indicated that approximately 25 percent of the d.c. input power to the pump oscillator was actually lost in the pump windings. Of this amount, very little was actually film loss since com-

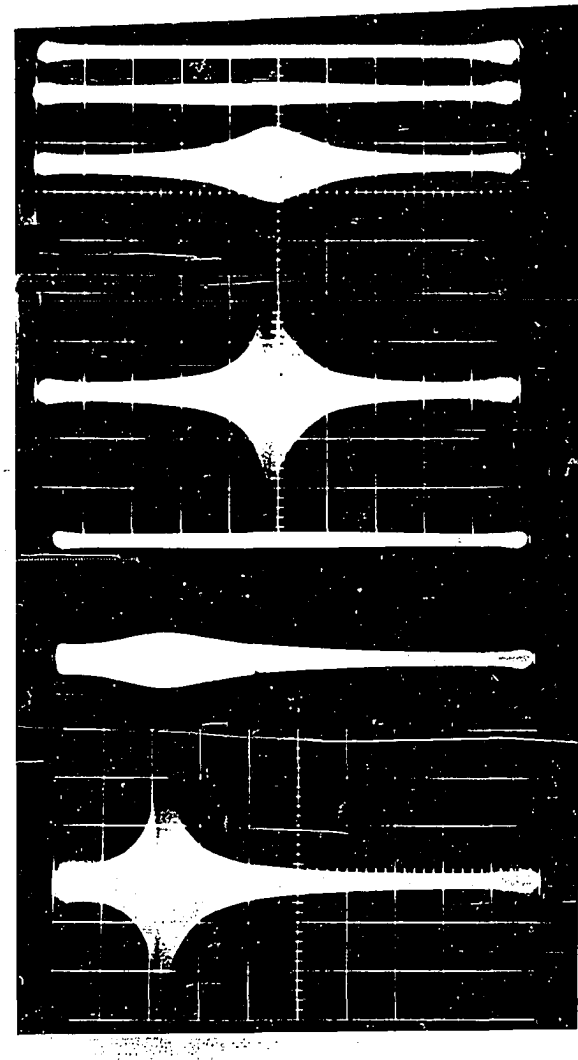

Fig. 16. The frequency response characteristic of the circuit of Fig. 15 for different pumping powers as indicated on Fig. 17 for C_4 = 0, a center frequency = 9.5 mc/s and a sweep rate = 50 kc/s per division

(A-D) R_L = 2700 ohms

(E-G) R_L = ∞

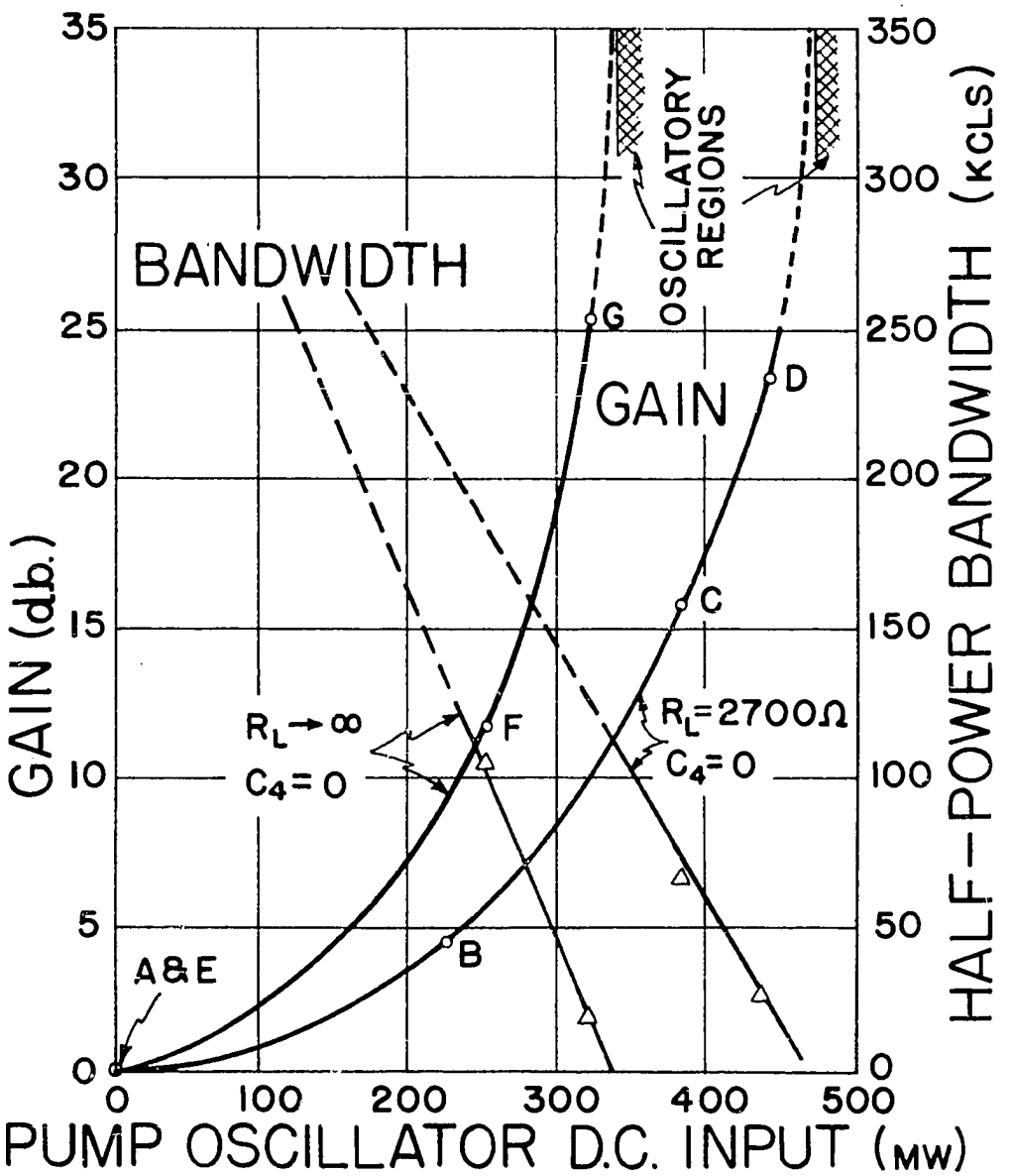

Fig. 17. Amplifier gain and bandwidth as a function of d.c. power input to the pump oscillator. The letters correspond to oscilloscope traces of Fig. 16

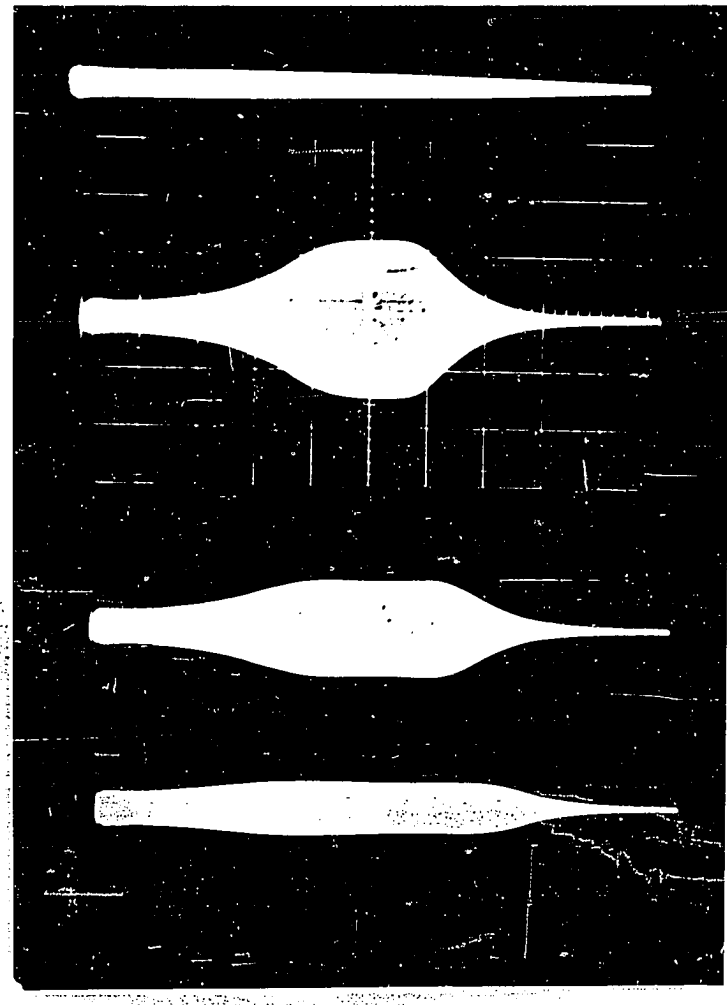

Fig. 18. The frequency response characteristic of the circuit of Fig. 15 for different d.c. bias currents, $R_L = \infty$, a center frequency = 9.5 mc/s and a sweep rate = 50 kc/s per division

(A) I_B = 20 ma (pump off)

(B-D) I_B = 20, 15 and 10 ma respectively (pump on)

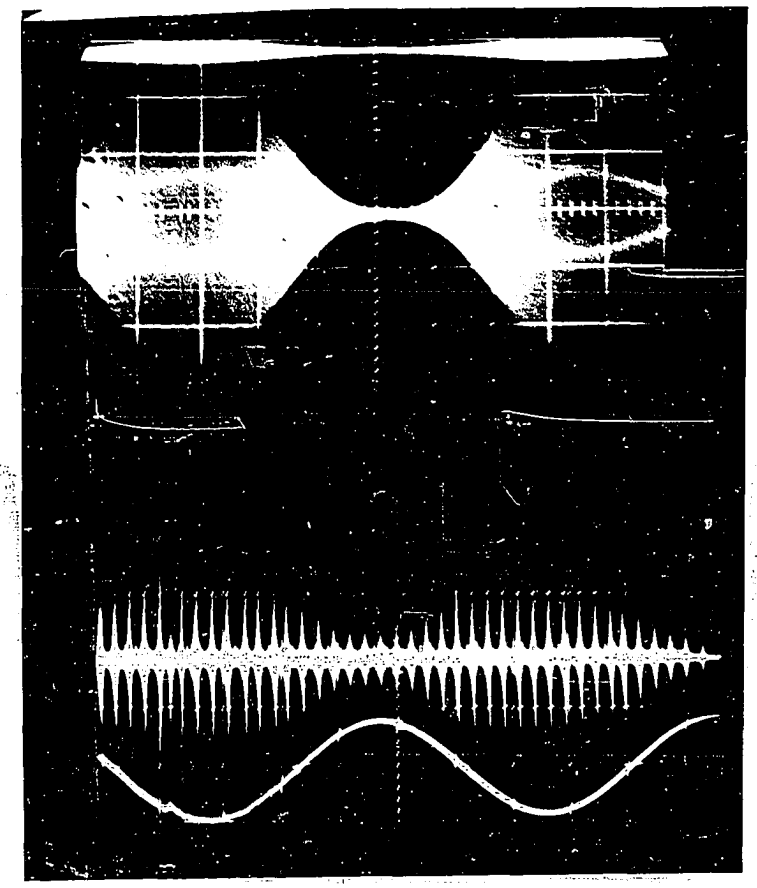

Fig. 19. The signal response of the two frequency parametric amplifier of Fig. 15 for a pump frequency of 26 mc/s

(A) The direct output (pump off) of a 10 mc/s carrier signal 100 percent modulated by a 500 cps modulation signal as illustrated in (D)

(B) The maximum possible stable conventional parametric amplifier gain of 22 db

(C) The 66 db gain and resultant output waveform with superregenerative amplifier operation and externally gated at 10 kc/s

plete removal of the transverse inductor had very little effect on the magnitude of the pump voltage. The low-level Q of the pump tank circuit was measured by the resonance curve method to be about 30.

Figure 18 shows an attempt to obtain a larger bandwidth than shown in Fig. 16. To accomplish this, C_3 was shorted out and C_4, C_2 and the mutual inductance of the transformer adjusted to give a response typical of an over-coupled i.f. stage. Next C_1 and C_3 were adjusted to give the response with pump power applied shown as Fig. 18(B). With pump power off, the response was that of Fig. 18(A). A decrease in the bias current changed the average value of signal winding inductance and thus the tuning of the system resulting in the responses of Figs. 18(C) and 18(D). The bias current, gain and bandwidths as measured from Fig. 18 are respectively 20 ma., 16.1 db and 130 kc/s for Fig. 18(B), 15 ma, 11.8 db and 195 kc/s for Fig. 18(C) and 10 ma, 6.9 db and 286 kc/s for Fig. 18(D). The center frequency of the sweep is 9.5 mc/s in each case with a sweep scale of 50 kc/s per division.

Some recent investigators (52, 53) have reported extremely high gains in using parametric amplifiers as superregenerative detectors. Figure 19 illustrates the operation of the two frequency amplifier previously described both as a conventional parametric amplifier and as a superregenerative amplifier. Figure 19(A) shows the 500 cps 100 percent modulated 10 mc/s output signal with the pump power off. When maximum pump power was applied so that the system was just short of oscillation, the output increased by about 22 db to that shown in Fig. 19(B). When the externally controlled modulation circuit x" - y" periodically varied the power supply voltage to the pump oscillator in a manner similar to that shown in Fig.

20(A), the pump oscillator output varied in a manner similar to that shown in Fig. 20(B). The voltage of the pump power supply was then adjusted so that when the pump oscillator output was a maximum, the signal circuit was oscillatory while at a pump output minimum the signal circuit was damped. When, in such a situation, the signal circuit changes from being damped to being oscillatory, the oscillation begins to grow from whatever initial conditions are present in the circuit at that time. If the initial signal conditions are large, the final amplitude reached after a fixed period of time is relatively larger than the final amplitude reached when the initial signal conditions are small. Within given limits the final signal is essentially a constant times the input.

In circuit operation of this type, an amplitude gain of several thousandfold can be obtained. With the same input as in Figs. 19(A) and 19(B), Fig. 19(C) represents such a case where the amplitude of the pulses represents a gain of approximately 66 db or a factor of 2000 over the output with the pump off. Figure 19(D) allows a comparison to be made between the waveform of the actual 500 cps modulation voltage fed to the signal generator and the final peak amplitudes of the superregenerative amplifier pulses.

The signal circuit of Fig. 15 was then considerably simplified so that it contained only the series combination of L_T, L_2 and C_3, all other elements except L_p being removed. The oscilloscope was then connected across L_T and the circuit tuned to one-half the pump frequency which was lowered to 24 mc/s. Figures 20(A) and 20(B) show the 25 kc/s modulation on the pump oscillator power supply and the oscillator output, while Fig. 20(C)

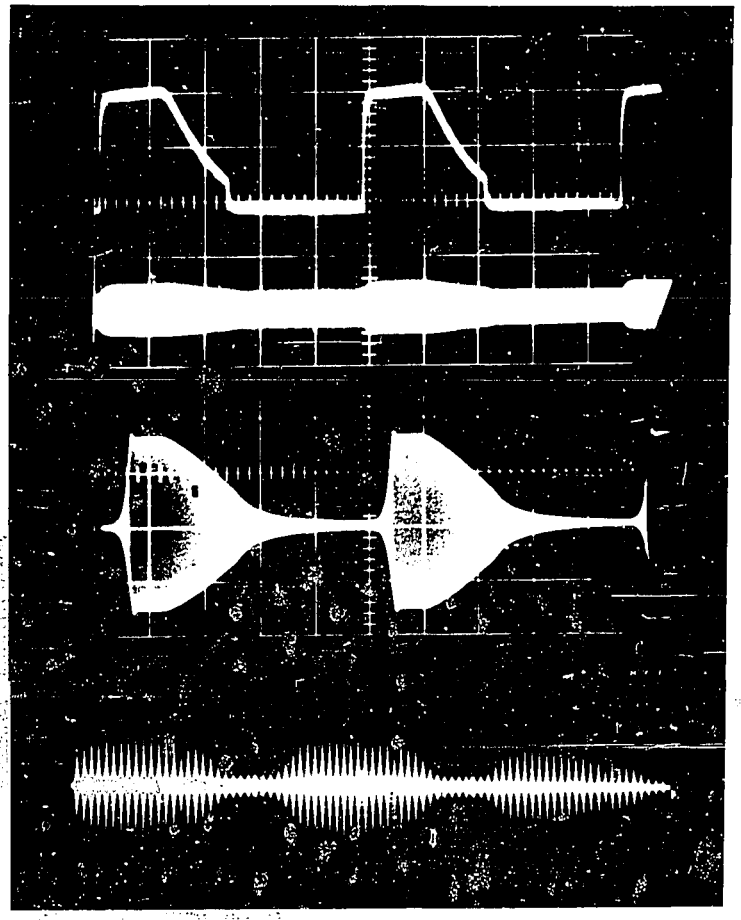

Fig. 20. The response characteristic of a degenerate superregenerative amplifier with a pump frequency of 24 mc/s

(A) The power supply modulation to the pump oscillator amounting to approximately 20 percent of total voltage

(B) The modulation on the output of the pump oscillator

(C) The growth and decay of the 12 mc/s parametron type oscillations for an excessive pump drive

(D) The superregenerative amplifier output for an external gate frequency of 25 kc/s and a 12 mc/s input signal modulated 120 percent by a 1000 cps modulation signal

shows a case of excess pump power resulting in extreme saturation in the signal circuit. The exponential build-up time of approximately five microseconds is readily seen. The operation of this circuit is identical to that of the parametron circuit described earlier. The rate of rise in this instance was considerably less than the case of the parametron however. In a properly designed system having a large gain per cycle and a large overall gain, such a circuit might prove useful as a simple receiver. Figure 20(D) illustrates the operation of a superregenerative detector giving approximately a 2000-fold gain for a 1000 cps 120 percent modulated input signal.

4. Summary comments on the thin film parametric amplifier

The thin film parametric amplifier has been analyzed on the basis of the lossless quasi-static model discussed in Section A. In order to analyze thin film parametric amplification at much higher frequencies, the losses in the magnetic material must be included. This means that the dynamic model of Fig. 4 must be used resulting in greatly increased difficulties of analysis as evidenced by the involved discussion on parametrons. To date no experimental work has been done using thin films as parametric amplifiers at anything other than with pump frequencies in the range of 10 to 30 mc/s. A further study of the parametric amplifier possibilities of thin films both with regards to operation in the several hundred megacycle per second region and with regards to the noise problems in such amplifiers is planned for the near future. Since thin films have not heretofore been used in devices of this type, little or no information is available concerning noise levels that might be expected. The physical systems used in

the experimental measurements presented in this thesis were not suitable for making good noise measurements. The whole question of noise generation in thin films is further complicated by the fact that there are many problems with regards to the ferromagnetism of the film itself that are not well understood.

At the present time one can not predict the practicality of thin ferromagnetic film parametric amplifiers in actual systems. Much will depend upon the results of the noise and the high frequency studies yet to be made and upon the development of a more optimum configuration for the film and the windings. One of the most difficult problems experienced was that of properly aligning the two windings and the film. The problem of alignment can be attacked in two ways. It is possible to evaporate films that have a much smaller anisotropy than the films used in the experiments described in this thesis. This would of itself make the system much less sensitive to alignment although some of the problem would still remain.

Another attack on the alignment problem would be to use a sandwich technique as shown in Fig. 21. In addition, low anisotropy films could also be used advantageously here. One of the windings could be etched on one side of a thin etched-circuit board and the other etched mutually perpendicular on the opposite side. The arrangement shown has a zero mutual inductance between the pump and the signal windings in the absence of any films. Capacitive coupling can be minimized by connecting the center tap on one or both windings to the ground plane of the overall system. Suppose that eight films are evaporated on a common substrate with their easy directions parallel to each other and to the center line of the output winding as illustrated in Fig. 21. Assume these eight films are

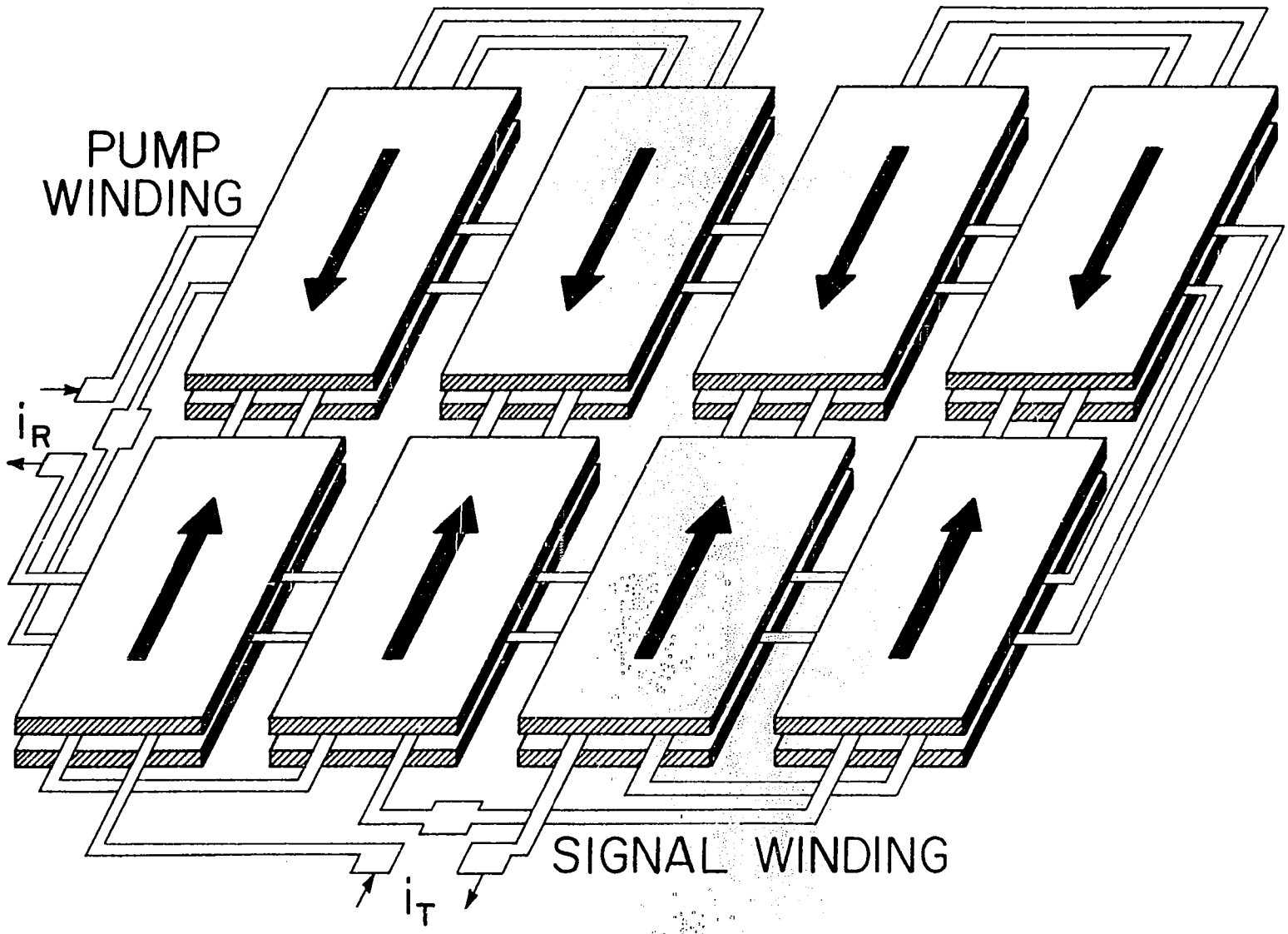

Fig. 21. A proposed thin film inductor using sandwich type construction

mounted film side down nearest the etched wiring with only a thin insulation separating the winding and the film and that eight more films are similarly placed on the under side. Since the two windings are mutually perpendicular to each other and fixed, the alignment procedure reduces to one where the films alone are moved. Once alignment is achieved, this sandwich could be encapsulated to make the alignment permanent. To provide shielding against stray magnetic fields the sandwich should be magnetically shielded by a high permeability material.

Since one of the reasons for the alignment was to reduce pump feedthrough and inasmuch as the alignment is determined by a physical orientation which can be expected to retain its placement even against rather severe mechanical and thermal conditions, a circuit element of this type promises to have many advanteges not presently available in many other systems.

A portion of the preceding discussion on the thin film parametric amplifier was presented as a conference paper and is presently in the process of being published in the Proceedings of the 1959 National Electronics Conference (54). A five column review of the conference paper was made by the editors of Electronics and published in the Research and Development Section of one of their recent issues (55).

D. A Thin Film Inductor as a Balanced Modulator

In the discussion of parametric amplifiers it was mentioned briefly in passing that a similar circuit might be useful as a modulator. The term modulator is used here to represent a device in which a low frequency signal is used to vary the amplitude of a carrier signal of much higher

frequency. Since all parametric amplifiers in the broad overall sense are modulators regardless of the relative frequencies of the two signals it is not surprising to expect the thin film inductor to also be useful as a modulator in the case where one frequency is much less than the other. In the discussion to follow it will be pointed out that if the windings and the film are properly aligned, then there will be no carrier frequency voltages induced in the output winding, the output voltage containing only the sideband frequencies. The possibility of a suppressed carrier sideband modulator in such a simple package merits consideration of the thin film inductor as a balanced modulator under a separate heading.

1. The balanced modulator circuit

Suppose a pair of mutually perpendicular windings are wound around the film with an alignment as shown schematically in Fig. 1(B) so that the axis of one winding, hereafter called the carrier rather than the pump winding as heretofore, is parallel to the rest direction of the film while the axis of the second winding, hereafter called the output winding rather than the signal winding as before, lies parallel to the transverse direction of the film. A modulation winding can be added in parallel with the output winding, or the output winding itself can be used as the modulation winding. It is to be noted that because of the mutually perpendicular orientation of the windings, no voltage is induced in the output winding if no currents flow in either the modulation or output windings.

A d.c. modulation input is somewhat easier to visualize than an a.c. input. At the same time it allows a simple qualitative description to be given which provides a good introduction to the balanced modulator oper-

ation. Consider Fig. 1 again. Suppose a d.c. bias current I_b and a single frequency carrier current i_c at an angular frequency of ω_c flows in the carrier winding and that a d.c. current flows in a separate modulation winding not shown in Fig. 1(B) but in parallel with the output winding. This current establishes a magnetic field in the transverse direction producing a torque on the magnetization vector $\vec{M}$ and causing it to rotate through an angle ϕ. This establishes a flux linkage in the output winding. Once $\vec{M}$ is rotated away from its rest position, the fields established by the a.c. carrier current in the carrier winding exert further forces on $\vec{M}$. These alternating forces cause the vector $\vec{M}$ to be rocked back and forth around some equilibrium value of ϕ, constantly changing the magnetic flux linking the output winding. This induces a voltage in the output winding at the frequency of the carrier and of an amplitude determined largely by the value of the equilibrium angle of rotation established by the amplitude of the d.c. current. Some nonlinearity with respect to modulation current is to be expected since this is a rotational phenomenon. This, however, can be kept small if the maximum angle of ϕ is kept small. A variable capacitor can be placed across the terminals of the output winding and the output circuit tuned to resonance. This permits at least partial suppression of carrier harmonics and increases the useful amplitude of the output.

A time varying modulation current slowly rotates $\vec{M}$ back and forth around the rest direction position while the carrier current rapidly rocks $\vec{M}$ around its equilibrium position. It is easy to see from this very qualitative description how a voltage such as the one shown in Fig. 22(G) for an actual experimental model can result. This is suppressed carrier double

sideband modulation.

With this qualitative picture in mind this problem may be analyzed somewhat more quantitatively. Reference to Eq. 52 shows that the voltage induced in the output winding contains among other frequencies, the sideband sum and difference frequencies of the carrier and the modulation components but no carrier frequency as such. In this case one associates the symbol for pump angular frequency ω_p with the symbol for carrier angular frequency ω_c, the latter symbol being used in the remainder of this discussion. Since the values of the a_n's for $n > 1$ are much smaller than a_1 for carrier amplitudes such that γ is in the order of 0.5 or less, Eq. 52 can be approximated as

$$e_T = L_o(1 + a_o/2) \sum_{m=1}^{\infty} I_m\omega_m \cos(\omega_m t + \theta_m)$$

$$+ \sum_{m=0}^{\infty} a_1 L_o I_m/2 \Big[(\omega_c + \omega_m) \cos[(\omega_c + \omega_m)t + \theta_m]$$

$$- (\omega_c - \omega_m) \cos[(\omega_c - \omega_m)t - \theta_m]\Big] \; ; \; \omega_{m_{max}} < \omega_c . \qquad 66$$

The output of the modulator can be taken as the voltage across the terminals of the output winding. It is evident that tuning the output circuit with a capacitor across the output terminals will reduce those sideband components of the harmonics of the carrier frequency that do exist. Furthermore, since the maximum modulation frequency in any practical system must be limited to values considerably below the carrier frequency, the first summation in Eq. 66 will normally be small compared with the second summation so that the second predominates for any reasonable magnitude of carrier amplitude. The

fact that the amplitudes of the two sidebands are somewhat different is of no real concern since this can be corrected by the gain-frequency characteristics of the amplifying stages that always follow such modulators.

The preceding analysis is based upon the premise that the two windings are mutually perpendicular to each other and that the axis of the carrier winding is exactly parallel to the rest direction of the magnetization. If this is not quite the case and the carrier winding axis is tilted somewhat from being parallel to the rest direction, a voltage at the carrier frequency will be induced in the output circuit even with no modulation signal present. By a suitable choice of an external magnetic field and/or rotation of the output winding, it is possible to find an equilibrium point where the zero-modulation induced carrier voltage in the output winding is again zero. The system, however, no longer has the simple symmetry of Fig. 1(B). Because of the anisotropy of the film, the equilibrium angle of rotation ϕ of the vector $\vec{M}$ will be different for a positive instantaneous magnitude of modulation signal than for a negative one of the same magnitude. Thus, unless the system is completely symmetrical as illustrated in Fig. 1 there will be a substantial carrier feedthrough into the output circuit with modulation and true balanced modulator operation will not occur. Any practical system utilizing this technique must therefore have a means for accurately aligning the two windings and the film relative to one another. A configuration similar to that of Fig. 21 appears to offer this possibility.

One of the anticipated advantages of permalloy films for application in balanced modulators is their relatively stable characteristics as a function of temperature. Although this has not been explored in great de-

tail, there is good reason to suppose that a modulator could be built having characteristics with negligible temperature coefficients, particularly with respect to carrier feedthrough, over the temperature range of at least from -100 to +100 degrees Centigrade. Furthermore the frequency characteristics of permalloy are such that one should be able to build modulators using permalloy films that operate with carrier frequencies from a few hundred kilocycles to at least several tens of megacycles per second.

2. Experimental verification of the thin film balanced modulator

The experimental verification of the feasibility of using thin film inductors as balanced modulators was made using the same film and windings as used in the amplifier investigation. The frequency of the transistor oscillator of Fig. 15 was lowered to approximately 12 mc/s. All circuit components connected to the transverse winding of Fig. 5 were removed and a variable tuning capacitor connected across the terminals. The ungrounded terminal of the transverse winding was connected through a 5600 ohm resistor to an audio oscillator which was used to supply the modulation current.

Using this circuit one can obtain both suppressed carrier and nonsuppressed carrier amplitude modulation. If the film and windings are deliberately misaligned, it is possible to obtain outputs resembling conventional amplitude modulation. Figures 22(A) and 22(C) illustrate such outputs, the first representing what is called a 100 percent modulated carrier while the second represents approximately 60 percent modulation. In each of these instances, the modulation signal had a frequency of two

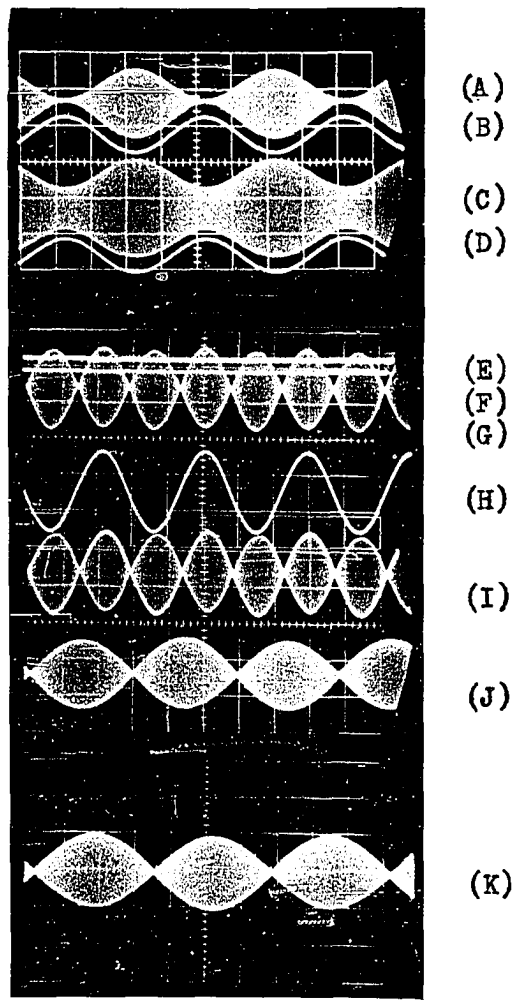

Fig. 22. Typical amplitude modulated output voltages from a thin film balanced modulator for sinusoidal modulation signals

kc/s. The waveform of the modulation signal is shown in Figs. 22(B) and 22(D).

When the windings and film bias were adjusted to give a minimum output with zero modulation, the residual output due to carrier feedthrough from stray coupling and the zero modulation signal were observed to be quite small as illustrated by Figs. 22(E) and 22(F). There is little difference between the oscilloscope trace widths in the two cases indicating that the carrier feedthrough was indeed quite low. Simple measurements indicated that even for this crude circuit arrangement, the output without modulation was at least 30 decibels lower than the output for a reasonable modulation signal. No measurement of carrier feedthrough with modulation could be made because of equipment unavailability. This, however, could be appreciable if the film and the windings are not correctly aligned so that the system is completely symmetrical about the rest direction of the film's magnetization.

Figure 22(G) shows a typical suppressed carrier double sideband output with the two kc/s sinusoidal modulation signal shown in Fig. 22(H). To illustrate the linearity of this thin film modulator, the oscilloscope traces of Figs. 22(G) and 22(H) were moved together to give Fig. 22(I). It can be seen that the envelope of the modulated waveform coincides very well with the waveform of the modulation signal.

Something of the wideband character of this type of modulator is illustrated by Figs. 22(J) and 22(K). The first of these shows the overlapping waveforms of the output and modulation signals for a 20 kc/s modulation frequency while Fig. 22(K) shows the same thing for a 20 cps modulation signal. The only adjustments made between Figs. 22(I), 22(J) and

22(K) was the frequency of the audio oscillator and the sweep speed of the oscilloscope. The magnitude of the output voltage of Fig. 22 was approximately two volts peak-to-peak throughout.

To check the possibility of using such a modulator as a radio frequency gating device and as a video modulator, a square wave generator was substituted for the audio oscillator used previously. Figures 23(A) and 23(B) again show the near zero output for a zero modulation signal input. Figure 23(C) shows the output waveform for the 100 kc/s square wave modulation signal shown in Fig. 23(D). Figure 23(E) shows the two traces moved together so that a better comparison of the two waveforms could be made. Lowering the amplitude of the modulation signal lowered the output accordingly as illustrated by Fig. 23(F). To illustrate that the modulation response is good even for low modulation frequencies, the 10 cps modulation and output are shown in Figs. 23(H) and 23(G) respectively. The ringing shown in Fig. 23(C) and 23(E) was a result of the transient due to the square wave current pulse in the output winding and was present whether or not the carrier was on. The amount of this ringing could be reduced relative to the output signal by a much tighter coupling between the output winding and the film. This could easily be the case in a circuit of more optimum design such as that proposed at the end of the amplifier discussion.

3. Summary comments on the thin film balanced modulator

The results of this early investigation were very encouraging indicating that a more extensive investigation should be made of this device. Mr. R. L. Samuels then proceeded to start such an investigation as a part of his Master of Science degree program. Although his work is still incom-

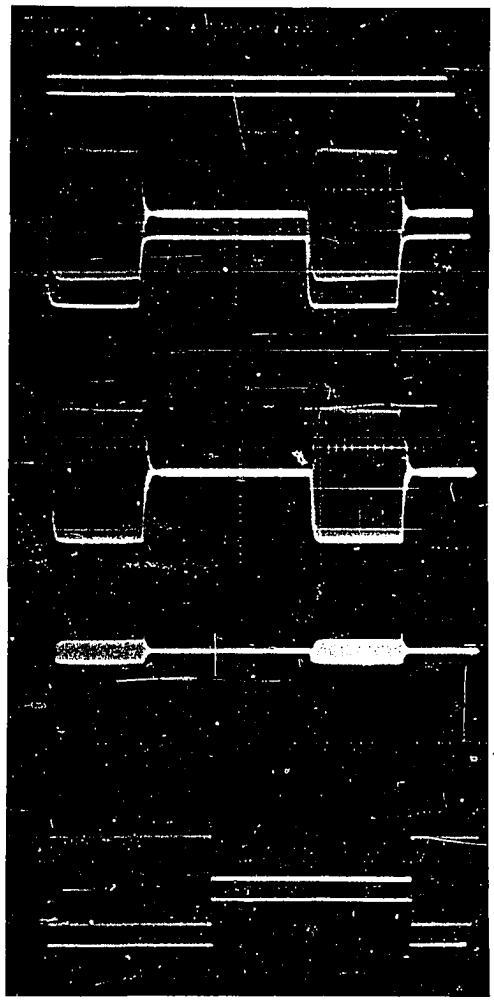

Fig. 23. Amplitude modulated output voltages from a thin film balanced modulator for square wave modulation signals

plete, Samuels' results to this writing have been quite successful and serve as much better confirmations of the feasibility of the use of thin film inductors in balanced modulator circuits than the experimental results presented above. For a more detailed study of the thin film balanced modulator, the reader is referred to Mr. Samuels' thesis which is scheduled to be deposited in the Iowa State University Library in the near future.

In view of the novelty and simplicity of this device, a paper describing its operation and the experimental results so far obtained was prepared by Samuels and this writer and presented in early February of this year before the 1960 Winter Convention on Military Electronics (56). This paper is to be submitted for publication in the near future. A four column summary of the paper was prepared by the editors of Electronics and published in the research and development section of one of their recent issues (57).

Balanced modulators are very widely used in radio communication equipment. Presently used schemes for obtaining suppressed carrier outputs are subject to many problems with regards to keeping the system in proper balance since they are in general quite sensitive to temperature and carrier amplitude changes. It is believed that these will not be serious problems in the thin film modulator although further study is required to check this. The generation of undesired harmonics is a problem encountered in balanced modulator work. This is not believed to be a serious problem either although this too must be checked experimentally. There is good reason to hope that in the final analysis the thin film inductor will be

found to be competitive with if not superior to the present methods for obtaining suppressed carrier amplitude modulated outputs.

Most of the discussion so far has more or less assumed that the modulation signal was continuously varying as would be the case for an audio or a video modulating signal. However, this need not be the case. If parametron logic circuits should ever prove feasible, then gate circuits that are in every aspect identical with what has been discussed here as the balanced modulator can be expected to find wide application as coupling units between and into and out of parametrons. In the case of a gate circuit, the modulation signal will be a rectangular gate pulse of either positive or negative polarity. It is easy to see that the phase of the output signal for a negative gate pulse will be exactly the negative of the output signal for a positive gate pulse, i.e., the two outputs will differ by exactly 180 degrees but will have the same amplitude. Some considerations of the use of a thin film balanced modulator as a gate in this manner is given in a paper already cited during the discussion of parametrons (50).

III. DISCUSSION

The investigation reported in the preceding pages concerns a new circuit element, the thin film inductor, which utilizes the single magnetic domain character of certain ferromagnetic materials when properly deposited in sufficiently thin layers. These thin film inductors possess some very exciting properties, some of which may prove of practical utility in the future. This circuit element can be used most effectively as a parametric device. The applications of thin film inductors to parametrons, to parametric amplifiers and to balanced modulators have already been discussed in some detail. These are related yet distinct applications of the same general circuit concept of a time varying reactance interacting with an input signal or signals to produce new but interrelated frequencies.

A number of other possibilities related to the ones already discussed in detail come to mind as being worthy of future investigation. One such possibility is the traveling wave parametric amplifier transmission line. Both the forward wave and the backward wave types would be of interest. Similar lines have been successfully constructed using variable capacitance diodes.

Another possibility for a new device is the utilization of the balanced modulator concept to design a frequency upconverting amplifier for the linear amplification of low level low frequency signals. The ultimate low level will depend upon the final results of the modulator studies. At present minimum current sensitivities of considerably less than a microampere appear reasonable. If perfected, such a unit should be very rugged and stable and could conceivably be used to replace galvanometer type de-

vices in many applications.

A third possibility that seems worthy of some initial investigation is a type of balanced modulator. Instead of a modulation current, however, one could conceivably use a magnetic field such as one finds in the vicinity of a magnetic recording tape. Used in the recording head of a tape recorder or similar device, the instantaneous output of the unit would be directly proportional to the instantaneous field intensity and would not be dependent upon the rate at which the tape was moving. Besides being potentially useful in conventional tape recording units, it could be used in the case of a thin film parametron computer to convert from a magnetic tape or drum memory directly to the parametron logic system at the frequency of parametron operation. The phase of this input would be either (+) or (-) depending only upon the magnetic polarity of the recording and not upon its speed past the reading head.

In addition to these, there are a number of other possibilities of application of thin films which may be impractical. There are undoubtedly a large number of other possibilities which have not yet been conceived but which may appear as investigation into the details of devices such as those described here proceeds. All in all thin film devices appear to be a fruitful area for future investigation. This is in addition to the study of the material properties of ferromagnetic films which must accompany any work of the device application type.

IV. BIBLIOGRAPHY

1. Kittel, C. and J. K. Galt. Ferromagnetic domain theory. In Seitz, F. and D. Turnbull, eds. Solid state physics. Vol. 3. pp. 437-557. New York, N. Y., Academic Press. 1956.

2. _____. Introduction to solid state physics. 2nd ed. New York, N. Y., John Wiley and Sons, Inc. 1956.

3. _____. Physical theory of ferromagnetic domains. Rev. Mod. Phys. 21: 541-583. 1949.

4. Dekker, A. J. Solid state physics. Englewood Cliffs, N. J., Prentice-Hall, Inc. 1957.

5. Blois, M. S., Jr. Preparation of thin magnetic films and their properties. J. Appl. Phys. 26: 975-980. 1955.

6. Conger, R. L. Magnetization reversal in thin films. Phys. Rev. 98: 1752-1754. 1955.

7. _____ and F. C. Essig. Resonance and reversal phenomena in ferromagnetic films. Phys. Rev. 104: 915-923. 1956.

8. Fowler, C. A. and E. M. Fryer. Magnetic domains in thin films of nickel-iron. Phys. Rev. 100: 746-747. 1955.

9. _____ and _____. Magnetic domains in thin films by the Faraday effect. Phys. Rev. 104: 552-553. 1956.

10. _____, _____ and J. R. Stevens. Magnetic domains in evaporated thin films of nickel-iron. Phys. Rev. 104: 645-649. 1956.

11. Olson, C. D. and A. V. Pohm. Flux reversal in thin films of 82%Ni, 18%Fe. J. Appl. Phys. 29: 274-282. 1958.

12. Smith, D. O. Static and dynamic behavior of thin permalloy films. J. Appl. Phys. 29: 264-273. 1958.

13. Gillette, P. R. and K. Oshima. Magnetization reversal by rotation. J. Appl. Phys. 29: 529-531. 1958.

14. _____ and _____. Thin film magnetization reversal by coherent rotation. J. Appl. Phys. 29: 1465-1470. 1958.

15. Kolk, A. J. and J. T. Doherty. Thin magnetic films for computer applications. Datamation 5, No. 5: 8-12. Sept.-Oct. 1959.

16. Pohm, A. V. and E. N. Mitchell. Magnetic-film memories: a survey. [To be published in Inst. Radio Engrs. Trans. on Computers ca. 1960.]

17. Landau, L. and E. Lifshitz. On the theory of the dispersion of magnetic permeability in ferromagnetic bodies. Physik Zeitschrift Sowjetunion. 8: 153-169. 1937.

18. Gilbert, T. L. and J. M. Kelley. Anomalous rotational damping in ferromagnetic sheets. Conf. on Magnetism and Magnetic Materials, Pittsburgh, Pa., June 14-16, 1955. New York, N. Y., Amer. Inst. Elect. Engrs. 1955.

19. Hartley, R. V. L. Oscillations in system with nonlinear reactance. Bell Syst. Tech. J. 15: 424-440. 1936.

20. Manley, J. M. and E. Peterson. Negative resistance effects in saturable reactor circuits. Trans. Amer. Inst. Elect. Engrs. 65: 870-881. 1946.

21. Landon, V. D. The use of ferrite-cored coils as converters, amplifiers and oscillators. Radio Corp. Amer. Rev. 10: 387-396. 1948.

22. Suhl, H. Proposal for a ferromagnetic amplifier in the microwave range. Phys. Rev. 106: 384-385. 1957.

23. Weiss, M. T. A solid-state microwave amplifier and oscillator using ferrites. Phys. Rev. 107: 317. 1957.

24. Bloom, S. and K. K. N. Chang. Theory of parametric amplifiers. Radio Corp. Amer. Rev. 18: 578-593. 1957.

25. _____ and _____. Parametric amplifiers using low-frequency pumping. J. Appl. Phys. 29: 594. 1958.

26. _____ and _____. A parametric amplifier using lower-frequency pumping. Proc. Inst. Radio Engrs. 46: 1383-1386. 1958.

27. Wittke, J. P. New approaches to the amplification of microwaves. Radio Corp. Amer. Rev. 18: 441-457. 1957.

28. Hogan, C. L., R. L. Jepsen and P. H. Vartanian. New type of ferromagnetic amplifier. J. Appl. Phys. 29: 422-423. 1958.

29. Heffner, H. Masers and parametric amplifiers introduction. 1958 Wescon Convention Record Part 3, (Electron Devices). New York, N. Y., Inst. Radio Engrs. 1958.

30. _____ and G. Wade. Gain, band width and noise characteristics of variable-parameter amplifiers. J. Appl. Phys. 29: 1321-1331. 1958.

31. _____ and _____. Parametric amplification. New York, N. Y., McGraw-Hill Book Co., Inc. 1960.

32. Wade G. Parametric amplification with solid-state material and with electron beams. Proc. Nat. Electronics Conf. (1959) 15: 46-57. 1960.

33. Tien, P. K. and H. Suhl. A traveling-wave ferromagnetic amplifier. Proc. Inst. Radio Engrs. 46: 700-706. 1958.

34. _____ and _____. Parametric amplification and frequency mixing in propagation circuits. J. Appl. Phys. 29: 1347-1359. 1958.

35. Manley, J. M. and H. E. Rowe. Some general properties of non-linear elements. Part I. General Energy Relations. Proc. Inst. Radio Engrs. 44: 904-913. 1956.

36. Rowe, H. E. Some general properties of non-linear elements. II. Small signal theory. Proc. Inst. Radio Engrs. 46: 850-861. 1958.

37. von Neuman, J. Non-linear capacitance or inductance switching, amplifying and memory organs. U. S. Patent 2, 815,488. Dec. 3, 1957.

38. Wigington, R. L. A new concept in computing. Proc. Inst. Radio Engrs. 47: 516-523. 1959.

39. Sterzer, F. Microwave parametric subharmonic oscillators for digital computing. Proc. Inst. Radio Engrs. 47: 1317-1324. 1959.

40. Goto, E. The parametron, a digital computing element which utilizes parametric oscillation. Proc. Inst. Radio Engrs. 47: 1304-1316. 1959.

41. Morecroft, J. H. Principles of radio communication. New York, N. Y., John Wiley and Sons, Inc. 1933.

42. Whittaker, E. T. and G. N. Watson. A course in modern analysis. 2nd ed. Cambridge, At the University Press. 1915.

43. McLachlan, N. W. Theory and applications of Mathieu functions. Oxford, At the Clarendon Press. 1947.

44. _____. Ordinary non-linear differential equations in engineering and physical sciences. Oxford, At the Clarendon Press. 1956.

45. Meixner, J. and F. W. Schäfke. Mathieusche Funktionen und Sphäroidfunktionen. Berlin, W. Germany. Springer-Verlag. 1954.

46. National Bureau Standards. Computation Laboratory of the National Applied Mathematics Laboratories. Tables relating to Mathieu functions. New York, N. Y., Columbia University Press. 1951.

47. Kotowski, G. Lösungen der Inhomogenen Mathieuschen Differential Gleichung. Z. Math. Mech. 23: 213-229. 1943.

48. Pohm, A. V., A. A. Read, R. M. Stewart, Jr. and R. F. Schauer. High frequency magnetic film parametrons for computer logic. Proc. Nat. Electronics Conf. (1959) 15: 202-214. 1960.

49. _____, _____, _____ and _____. Operation of magnetic film parametrons in the 100 to 500 mc region. [To be published J. Appl. Phys. Supplement to April Issue Vol. 31. 1960.]

50. _____, _____, _____ and _____. Some applications of magnetic film parametrons as logical devices. [To be published in Inst. Radio Engrs. Trans. on Computers ca. 1960.]

51. Morse, T. Logical design of a three-state adder stage. Unpublished M. S. Thesis. Ames, Iowa, Library, Iowa State University of Science and Technology. 1960.

52. Bossard, B. Superregenerative reactance amplifier. Proc. Inst. Radio Engrs. 47: 1269-1271. 1959.

53. Younger, J. J., A. G. Little, H. Heffner and G. Wade. Parametric amplifiers in superregenerative detectors. Proc. Inst. Radio Engrs. 47: 1271-1272. 1959.

54. Read, A. A. and A. V. Pohm. Magnetic film parametric amplifiers. Proc. Nat. Electronics Conf. (1959) 15: 65-78. 1960.

55. _____ and _____. Parametric amplifier uses thin films. Electronics 32, No. 46: 92-94. Nov. 13, 1959.

56. _____ and R. L. Samuels. Thin ferromagnetic film balanced modulators. Paper presented at 1960 Winter Convention on Military Electronics, Los Angeles, Calif. Mimeo report Feb. 5, 1960.

57. _____ and _____. Thin film balanced modulator. Electronics 33, No. 9: 78-80. Feb. 26, 1960.

V. ACKNOWLEDGEMENTS

The writer wishes in this space to acknowledge the debt of gratitude he owes to the many many persons, teachers and instructors in particular, who have over these many years been instrumental in aiding him to reach the point of writing this thesis. To his wife and family he owes a special debt for the many hours spent "busy being a student". With regard to this thesis, he wishes to thank Dr. A. V. Pohm who suggested a study in this area, Dr. W. B. Boast for his interest and support and the many others who gave helpful advice and encouragement. He also wishes to thank Mr. W. T. Lewish and Dr. E. J. Schweppe for their help in programming the Cyclone and Mr. R. D. Anderson for the excellence of the drawings. It is a pleasure to acknowledge the help in the form of fellowships which have been received from the Bendix Aviation Corporation and the National Science Foundation. The help of Mrs. Beulah Lande Erickson in the final preparation of this thesis is most gratefully acknowledged.